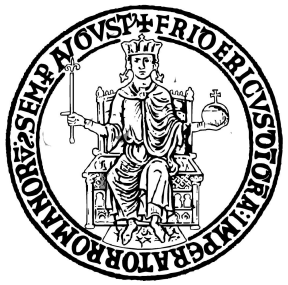

Università degli Studi di Napoli "Federico II"

Corso di Dottorato in FISICA

Ciclo XXXI

Coordinatore: Prof. Salvatore Capozziello

Study of effects induced by a nuclear stratosphere upon statistical particle emission processes

Dottorando:

Federico Davide

Tutori:

Prof.Emanuele Vardaci

Dr. Antonio Di Nitto

Anno Accademico 2015/2018

Contents

Introduction

The models of nuclear structure that describe reasonably well the proprieties of the atomic nuclei which are located in the valley of stability and in the region close to it provide unusual properties for nuclei far from this. Essentially these nuclei may have properties that differ significantly from those of nuclei at the stability valley and for this reason they are called exotic. Mass, radius, spin, magic numbers follow trends very different from those of stable nuclei. The various attempts to extrapolate the properties related to the nuclear structure far from stable region lead to predictions very different depending on the theoretical models used. This aspect becomes more apparent as we start to explore what is called the " terra incognita". Typical characteristics of these nuclides such as low production cross sections and relatively short lifetimes make complicated the production and study. Employing stable ion beams and exploiting the characteristics of certain types of reactions it is possible to explore specific areas of the nuclide chart. Transfer reactions for instance allow to move a little away from the valley of stability, fusion-evaporation reactions create proton-rich systems, while deep inelastic collisions, as fission, allow to produce neutron-rich nuclei. One can also use beams consisting of unstable ions in order to explore the properties of exotic nuclei both from the point of view of the structure and the dynamics of reaction.

The production of exotic nuclei, beam stable and unstable, however, needs a preparatory study in order to predict cross sections and the kinematics of the reaction products to optimize significantly the rates of production. The exotic nuclei produced are typically excited and their de-excitation occurs through the emission of light particles and gamma rays. One of the tools used to study nuclear evaporation is the Statistical Model of evaporation. However, the Statistical model, despite being a powerful tool, is not always able to reproduce the physical observables of interest in an optimal manner.

Numerous articles in the late 80s and early 90s have, in fact, highlighted some gaps in the predictive power of the same in extreme conditions. In the case, for example, of hot nuclei, it is sometimes necessary to use different parametrizations to reproduce the data of each specific emission channel investigated. Often the reproduction of the data is only possible after the measurements are performed and with unrealistic parametrizations.

The main objective of this work is therefore to try to make up for missing ingredients in the statistical model by introducing an element dependent on these extreme conditions and apply the acquired knowledge to explore the region of the " terra incognita" . We will then investigate the model of the nuclear stratosphere proposed by Batko and Civitarese using it in the statistical model and analyzing the simulated physical observables. In this way we can understand how the nuclear stratosphere model influences the latter. Once this is done, we will use the knowledge acquired to replicate some experimental data where the statistical model fails to verify the goodness of the stratosphere model used.

Chapter 1

Evaporation and Statistical Model

In the quest for the production of new elements, heavy-ion beam accelerators were developed starting from 1950. The use of these facilities made the discovery of elements in the regions of the nuclear chart corresponding to the exotic nuclei. If properly accelerated, a heavy-ions fuse with target nuclei and generate compound nuclei that decay by the emission of light particles and gamma rays by populating new nuclei. This process, called fusion-evaporation, is not only an excellent tool to efficiently produce new elements, but it is also the most productive reaction mechanisms to discover new nuclides.

Under specific conditions, the interaction between projectile and target can favor faster processes in which the formation of the compound nucleus does not take place, for which it is preferable to use more advanced models which are able to reproduce the other competing reactions as well. However, in reactions involving light ions, it is possible to simplify the problem, since the production of compound nuclei are uninfluenced by the dynamics in the input channel. Models have been developed to predict the cross sections of the different channels, the angular and energy

distributions of the reactions products and the evaporated particles, as well as the multiplicities of these latter. They generally offer a good reproduction of the physical observables. Although much work has been devoted to fusion-evaporation, there are still open questions. They mainly refer to the limitation of the standard parametrization included in the statistical model to reproduce the behavior at high excitation energies or at high angular momentum. In this chapter, we will briefly recall the basic physical concepts underlying compound nucleus formation and decay. Then we will check several interesting works on fusion-evaporation performed with the SM and we will end by addressing several open questions on the fusion-evaporation that show the quest for new physics.

1.1 Fusion Reaction or CN formation

Reactions that involve heavy ions, with energy in the center of mass higher than the Coulomb barrier, have the wavelength of DeBroglie associated to the relative motion projectile-target smaller than the dimensions of the two colliding nuclei. So it is possible to ignore the quantum aspects of the problem and examine the motion of the colliding nuclei using a classic approach. Different types of processes generated under this condition can be classified as function of the impact parameter b, i.e depending on the orbital angular momentum $l\hbar$ of the entrance channel. According the semi-classical relation :

$$l\hbar = \mu P_\infty b$$

where P_∞ is the asymptotic linear momentum and μ is the reduced mass of the system. The reaction cross section σ_R can be expressed in terms of l

$$\sigma_R = \frac{\pi}{k^2}\sum_{l=0}^{\infty}(2l+1)T_l$$

where T_l represents the probability that the reaction takes place and k is the wave number of relative motion. Using the approximation of sharp cut off for T_l , we obtain the expression

$$\sigma_R = \frac{\pi}{k^2}(l+1)^2$$

Differentiating with respect to l, we get

$$\frac{d\sigma_R}{dl} \approx \frac{2\pi}{k^2}l$$

Within this formalism we can classify reaction using the orbital angular momentum.

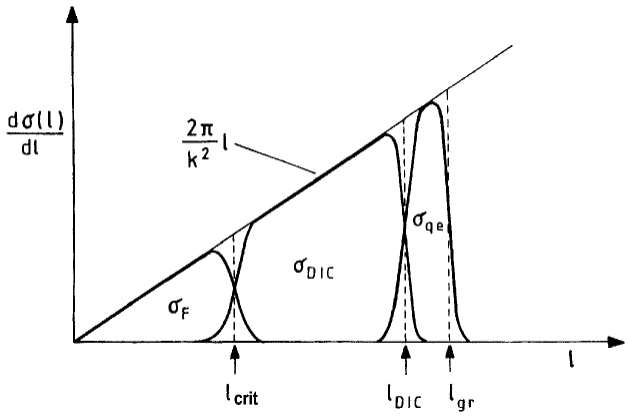

Figure 1.1: Reaction cross section as a function of the orbital angular momentum. The different types of reactions can be classified as function of l : from 0 up to l_{crit} we have the fusion reactions , than deep inelastic collision and from l_{DIC} to l_{gr} the Quasielastic reactions.

Large values of l produce the most peripheral reactions such as the deep inelastic or direct reactions while complete fusion reactions take place at l lower than l_{cr}[1], where the large overlap of density of nuclear matter of projectile and the subsequent thermalization of the system produces the CN formation.

1.2 CN Decay or Evaporation Residue Channel

In fusion reactions the CN formation represents the intermediate step preceding the de-excitation of the system and can be expressed as

$$x + A \rightarrow CN^*$$

where x and A are the projectile and the target nuclei, respectively. The CN is characterized by an excitation energy E^* and by an angular momentum J. The excitation energy E^* of the system is given by the sum of the Q value for the formation of compound nucleus $Q = m_x c^2 + m_A c^2 - m_{CN} c^2$ where m_x,m_A and m_{CN} are the mass of projectile, target and compound nucleus, respectively, and E_{rel} is the kinetic energy of the relative motion in the center of mass

$$E^* = E_{rel} + Q$$

The entire kinetic energy of relative motion is dissipated through a series of nucleon-nucleon interaction inside the system. The excited configuration of the CN is not stable due to the excitation energy and angular momentum, therefore it can survive for timescales typically in order of $10^{-21}s$. The main decay processes are: particles evaporation and fission. Accordingly to the *Bohr'independence hypothesis* of the CN,

[1] we define l_{cr} as the maximum value for complete fusion

we consider the decay of CN independent from its formation process; so the system loses memory of his formation channel but it conserves energy, angular momentum and parity. The CN decays mainly by the evaporation of light particles, fission and gamma emission. The cross section of each reaction channel can be calculated as the product of the fusion cross section of the colliding ions σ_{fus} and the probability of the excited CN in a specific decay channel (b) G_{ev} of the exit channel

$$\sigma_{a\to b} = \sigma_{fus} G_{ev}$$

In the region of low excitation energy, where an isolated state is populated, this cross section is described by the Breit-Wigner formula [Hog78]. At high energy, instead, the spacing between the nuclear levels is reduced and at the same time their width increase so it is not longer possible to use the Breit-Wigner formula because their widths overlaps. Hence, it is necessary a treatment based on a statistical approach in order to describe the decay of the CN.

1.2.1 Evaporation of light particles

In the first stages of the CN de-excitation mainly light particles, such as neutrons, protons and α-particles are emitted. They remove larger amount of excitation energy and angular momentum. When the excitation becomes lower and lower the emission probability of γ- rays increases. In fact the emission probability depends on the atomic number, excitation energy and angular momentum of the CN and on mass and charge of the emitted particle. The excitation energy of the CN can be separated in two terms:

$$E^* = E_{th} + E_{rot} \tag{1.1}$$

where E_{rot} is the collective rotational energy and E_{th} is the thermal energy related to the random motion of the nucleons. Rotational energy is related to the angular momentum $\vec{J}$ by the following equation

$$E_{rot} = \frac{|\vec{J}|^2}{2\mathcal{I}} \tag{1.2}$$

where $\mathcal{I}$ is the moment of inertia of the CN that, in the rigid sphere approximation, can be calculated as

$$\mathcal{I} = \frac{2}{5}MR^2$$

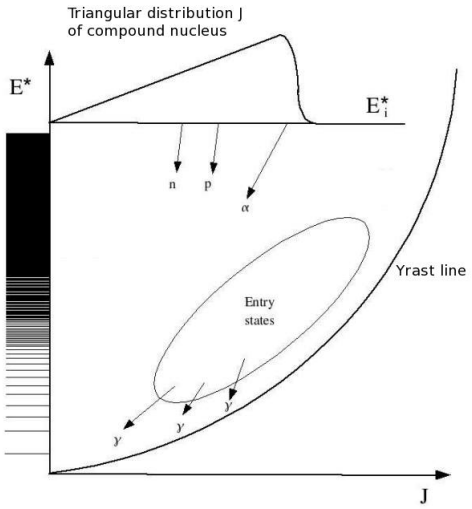

Figure 1.2: $E^* - J$ plane. At the top of the graph is a schematic the triangular distribution of angular momentum of the initial compound nucleus. The yrast line is relative to a possible spherical rigid rotator as an evaporation residue.

The Yrast line, in Fig. 1.2, in the $E^* - J$ plane is a curve that represents a cooled rigid rotator in which all the excitation energy is stored only in the collective rotational motion. Under the yrast line the value of the excitation energy E^* would

be smaller of the rotational energy, hence no nucleus of a given angular momentum can exist below the yrast line. Using the $E^* - J$ plane it is possible to draw a schematic description of the decay of the CN from its formation to the ground state of the residual nucleus. As it can seen in the Fig. 1.3 the nucleus is initially in an excited state of energy E^* in the continuum region and has an angular momentum J_i.

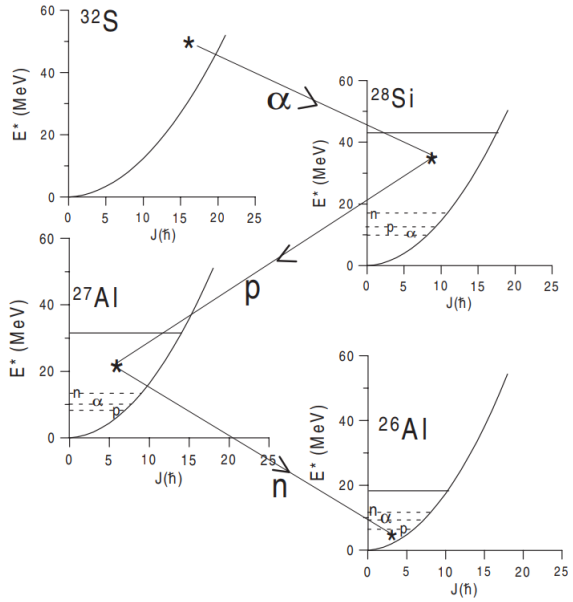

Figure 1.3: Multistep evaporation (evaporation cascade) from the compound nucleus ^{32}S. The continuous horizontal lines indicate the maximum excitation energy E^*_{max} which could be reached in each daughter nucleus, and the n, p and α-particle thresholds are shown as dashed horizontal lines. The cascade stops when the point reached in the E^*–J plane lies below the lowest particle emission threshold, in which case the evaporation residue ^{26}Al decays by gamma rays to the ground state. For heavy nuclei, gamma decay competes significantly even above the particle emission thresholds.

The CN decays preferably by emission of light particles rather than electromagnetic radiation emission. Each particle carries away part of excitation energy and

part of angular momentum moving in the $E^* - J$ plane bottom left. After each emission the energy of the residual nucleus is given by

$$E_f^* = E_i^* - Q_s - \varepsilon$$

and the angular momentum

$$\vec{J_f} = \vec{J_i} - \vec{l}$$

where E_f^* and E_i^* are the final and initial excitation energy, respectively. Q_s is the separation energy of the emitted particle, ε is the kinetic energy of emitted particle , J_f and J_i are the initial and final angular momentum while l is the angular momentum carried away by the emitted particle. The process continues with further emissions until the excitation energy and angular momentum are enough for particle emission. Electromagnetic transitions proceed towards the Yrast line through a statistical cascade and eventually with a sequence of Yrast states towards the ground state. The final nucleus originated in this chain of processes is called *Evaporation Residue* (ER).

1.2.2 Particle evaporation probability

In the statistical model the *Bohr's independence hypothesis* and the *principle of detailed balance* are invoked in order to relate the transition probability from the initial state to the final state with the transition probability of the inverse process, namely from the final state to the initial state. It is possible to demonstrate that the emission probability of a particle i with energy ε_i and angular momentum l_i from a

CN with angular momentum J_0 and excitation energy E_0 is given by [Eri60, Dos77]

$$P_i(E_0, J_0, (\varepsilon_i, l_i), E_{ER}, J_{ER}) \propto \rho(E_d, J_d) T_{l_i}(\varepsilon_i) \tag{1.3}$$

where E_d and J_d are energy and angular momentum of the daughter nucleus after the emission of the particle i; $\rho(E_d, J_d)$ is the level density of the daughter nucleus and $T_{l_i}(\varepsilon_i)$ is the transmission coefficient of the fusion of the particle i with the daughter nucleus in order to create the compound nucleus (the inverse process). The equation 1.3 has to be normalized to the total emission probability:

$$P_{tot}(E_0, J_0) = \sum_i \sum_{l_i} \sum_{J_1=J_0-l_i}^{J_1=J_0+l_i} \int P_i(E_0, J_0, (\varepsilon_i, l_i), E_i, J_i) d\varepsilon_i$$

Because the entire process of decay is governed by the 1.3 normalized, both transmission coefficients and level density acquire an essential role.

1.2.3 Level density

The level density ρ in the formula 1.3 accounts for all the single particle states accessible with energy and angular momentum given A and Z of the nucleus. Considering that the decay are considered for nuclei in the continuum region, this level density can be calculated throughout different ways in which the nucleons of the system can be disposed in the states of single particle in order that the total energy of the system is within the range E, $E + dE$. The determination of the states of single particle can be resolved starting from the adoption of a nuclear model. In case of high excitation energies, when spacing between the nuclear levels decrease and their width increase, a statistical method is applied. We can use a grand partition function that describes the statistical properties of a system in thermodynamic equilibrium.

If the nucleus can be considered as a Fermi gas, or an ensemble of a large number of non-interacting fermions, the energetic levels of single particle can be assumed equally spaced. So, starting from the assumption that the compound nucleus is a system of non-interacting fermions, it is possible to obtain the expression of level density for the CN [Eri60] :

$$\rho(E*,J) = \frac{2J+1}{24}\sqrt{a}(\frac{\hbar^2}{2\mathcal{I}})^{\frac{3}{2}}(E^* - \frac{\hbar J(J+1)}{2\mathcal{I}} + \triangle E)^{-2}* \tag{1.4}$$

$$*exp\left\{2\left[a\left(E^* - \frac{\hbar J(J+1)}{2\mathcal{I}} + \triangle E\right)\right]^{\frac{1}{2}}\right\}$$

where J is the angular momentum of the given nucleus, a is the level density parameter and $\mathcal{I}$ is the moment of inertia of the nucleus. The parameter a, sometimes called the " little a" can be chosen, approximately, in the range $\frac{A}{10}\ MeV^{-1} \leq a \leq \frac{A}{7}\ MeV^{-1}$ for nuclei width mass $A < 100$ and in the range $\frac{A}{11}\ MeV^{-1} \leq a \leq \frac{A}{8}\ MeV^{-1}$ for nuclei width $A > 100$. As we can see in the Fig.1.4 the trend of the a value as function of the mass A follows a straight course except very specific case mainly due to shell effects.

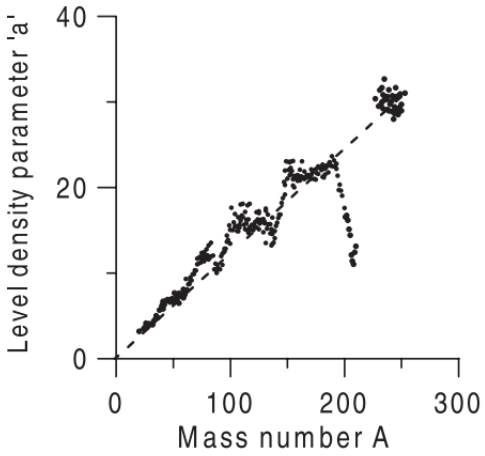

Figure 1.4: a parameter values in fuction of mass number A. The dotted line represents $\frac{A}{8}$

1.2.4 Transmission coefficient

The second term of 1.3 is the transmission coefficient of the absorption of a light particle from a residual nucleus. We known that in the interaction between nuclei both repulsive and attractive forces compete with each other. The attractive forces produce absorption effects that can be evaluated through the use of a complex potential. In analogy to the complex formulation of the refractive index in optics, it is possible to add an imaginary term to the nuclear potential in order to obtain what is defined as optical potential

$$V_{opt} = V(r) + iW(r)$$

that once replaced in the Schrödinger equation gives

$$(-\frac{\hbar^2}{2\mu}\nabla^2 + V_{opt}(r))\Psi(r) = E\Psi(r)$$

At this point, the divergence of the probability density currents is calculated

$$\nabla \cdot \mathbf{j} = \frac{\hbar}{2\mu i}(\Psi^* \nabla^2 \Psi - \Psi \nabla^2 \Psi^*) \tag{1.5}$$

The absorption cross section is defined as the ratio between the net probability density current (that is the difference between the ingoing and outgoing current) and the probability current of the incident wave

$$\sigma_{abs} = \frac{\triangle j}{j_{in}} \tag{1.6}$$

we can rewrite this using 1.5 as :

$$\sigma_{abs} = \frac{\pi}{k^2} \sum_l (2l+1)(1 - |S_l|^2)$$

where $1-|S_l|^2$ are the transmission coefficients usually indicated with T_l. $S_l = e^{i2\delta_l}$ is the scattering matrix and δ_l is the "phase shift" derived by the presence of a potential $V(r)$. In the case of a real potential, δ_l is a real quantity, but if there is an imaginary part of the potential also δ_l has an imaginary part. In this way it is easier to see the transmission coefficients as the probability that a particle i produces inelastic process but above all we note the strong dependence of the transmission coefficients on the definition of the optical potential used. For the case of strong dominance of the fusion process T_l represents with good approximation the transmission coefficient that has to be used in the equation 1.3.

The transmission coefficients are extracted from several reactions involving the incoming particle and the daughter nucleus by means of the optical model. However, these reactions have been investigated experimentally for target nuclei in their ground states and all parameters of the OM potentials are for *cold nuclei at low spin*. It

is expected that the deformation of the compound nucleus such as predicted by the RLDM, modifies the evaporation barrier (and therefore the TC).

1.3 The SM for the study of fusion-evaporation

Since decades from its first formulation [Hauser-Feschbach] the statistical model represents the most powerful tool to investigate the evaporative decay of excited nuclei. This approach allows to provide a good reproduction of the physical observables characterizing the process that are usually accessible in experiments, e.g. cross sections and particle multiplicity, energy and angular distributions. The model prescriptions commonly used are based on systematics collected in the surrounding of the valley of stability. In fact, these nuclei are the most simple to access with existing beam/target combinations. However, it is of large interest to provide more global prescriptions able to predict the behavior of the more exotic nuclei rarely populated or accessible with radioactive beam facilities under construction. A better knowledge of these nuclei it is relevant not only to improve the knowledge of the nuclear matter in extreme conditions but also to provide a more reliable description of the processes relevant in the astrophysical environments. A good starting point in the direction of this long-range plan requires to solve the discrepancies between data and predictions observed in the last decades in the region around the valley of the beta-stability in the region of relatively high excitation energies and angular momentum where the fission decay contribution is still negligible.

In the following paragraphs, we will show three different reactions whose observables cannot be reproduced by the well-established parametrizations considered in the SM codes. In order to overcome these lacks, we propose the use of alternative prescriptions for the distribution of nuclear matter in the CN that is based on the

nuclear stratosphere model [Bat88]. Using this model new analyses of existing data on three reactions were carried out and the very promising results are described in the following chapters.

1.3.1 Appearance of non-spherical emission in light systems (Single-step VS Multistep codes)

An early work by La Rana et al., using ^{40}Ar + ^{27}Al reaction at Elab= 190 MeV [Lar87] evidenced the limits of the physical ingredients usually considered in the SM for the description of the evaporation channel. They have measured energy spectra and angular distribution of protons and α-particles. The composite system $^{67}Ga^{*}$ was formed at an excitation energy of 91 MeV, and the critical angular momentum for fusion J_{ER} is $\backsim 46\hbar$ as derived from fusion cross-section data.

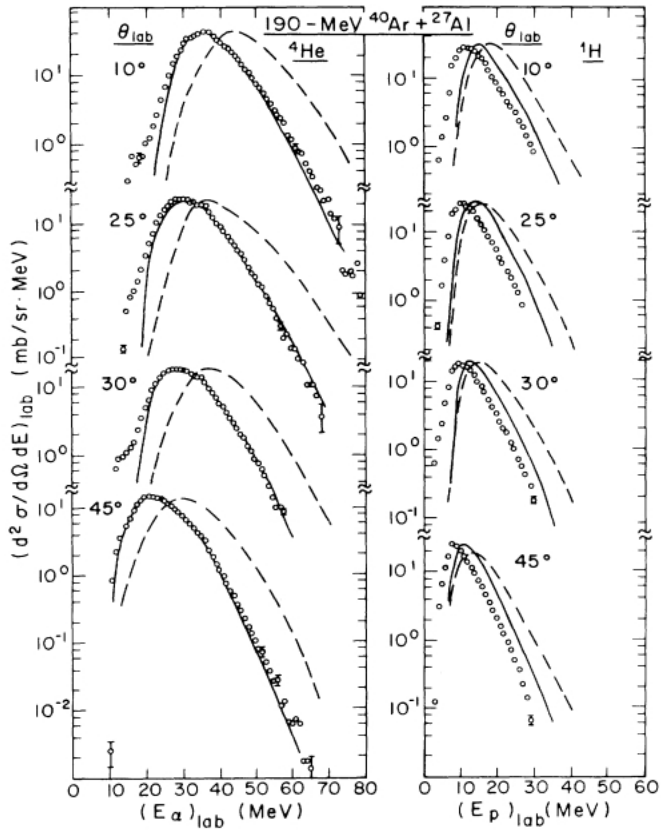

Figure 1.5: Energy spectra of α-particles (left) and protons (right) for various detection angles. The points are experimental data and the curves are statistical model calculations for spherical nuclei (dash line) and deformed nuclei (solid line).

From the experimental point of view, the study was based on the measurements of the protons and α-particles. The authors evidenced experimental energy protons and alpha particle spectra shifted at lower energy with narrow widths with respect to those simulated by assuming the evaporation from a spherical nucleus, as shown in Fig.1.5. At the same time also the angular distributions of both particles show anisotropies much smaller than experimental ones, see Fig.1.6.

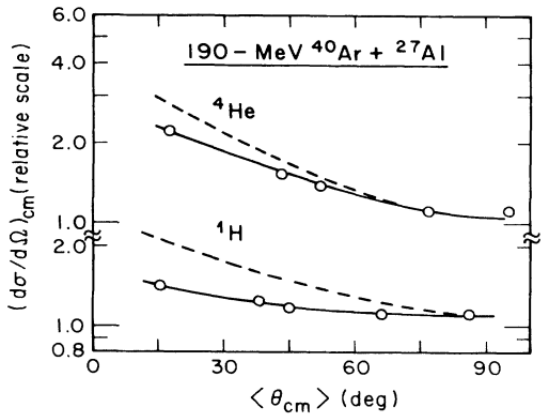

Figure 1.6: Angular distributions of α-particles and protons in c.m system. The points are experimental data and the curves are statistical model calculations for spherical nuclei (dash line) and deformed nuclei (solid line). The calculated curves have been normalized to the data at 90° to illustrate the difference in anisotropies.

Therefore the experimental trends of this set of observables seems to indicate the presence of deformations in emitting nuclei much larger than those predicted by the RLDM [Coh74]. Therefore the reproduction of the experimental data required to consider very large deformations. We have to note that emission from elongated nuclei requires to take into account not only the reduction of emission barriers but also the increase of the moment of inertia. These effects are consistently implemented in the computer code GANES based on the SM model [Aij86]. This model allows to simulate the emission of light particles from nuclei with different axially symmetric shapes. The code uses the Cassinian ovals [Paschevic] to describe the charge distributions for different nuclear shapes: prolate, oblate and pear-shaped as well as spherical. Furthermore the TC can be modified using different barrier heights for the light particle emission. Both these quantities modify the energy and spatial distribution of light charged emitters, therefore allow to put strong constraint on the

nuclear shapes. Considering deformations corresponding to an axis ratio $\frac{b}{a} = 2.4$ the α particle spectra, at different laboratory angles, as well as the proton and α particle angular distributions were simultaneously reproduced, see Fig.1.5 and Fig.1.6. The protons spectra were calculated with the same deformed shape and effective excitation energy as were used for α-particles spectra but the predicted spectra are still at significantly of higher energies than those observed. Larger deformations are needed. Hence, this behavior indicates that the emission of light charge particles occurs from peripheral regions of the nuclei, but the simple assumption of large deformation is unrealisitic. It seems to be lacking an ingredient that increases the average evaporation radius but is not obtainable through symmetrical deformation. Probably some basic features are missing in the statistical model description.

1.3.2 Confirmation of nuclear deformation (Single-step VS Multistep codes)

The indications emerging from the work of La Rana et al.[Lar87] were immediately confirmed the subsequent year by measuring the α-particles produced in the reaction 120 MeV ^{30}Si + ^{30}Si[Lar88]. Also in this work a large discrepancy between the measured α-particles spectra and the simulated ones, assuming spherical nuclei, were observed. The measured α-particles energy spectra were much softer than the simulated one (shifted at higher energy and significantly broader) when emission from spherical nuclei with $J_{ER} = 38\ \hbar$ and the emission barrier from the fusion systematics were assumed. To overcome the discrepancy with the experimental data much smaller values of the emission barrier and much smaller values of the J_{ER} have been used. Therefore the data suggested that the emission is mostly from deformed nuclei and elongated shapes with a major to minor axes ration $\frac{b}{a} \approx 3$ (the so called hy-

perdeformation) were needed to reproduce the data. The presence of a similar effect observed in the decay of a CN with different asymmetry in the entrance channel should exclude as origin effects due to direct reactions, i.e. processes taking place before the complete thermalization of the composite system. Such conclusions are also confirmed by the comparison of the invariant differential cross sections measured at forward and backward angles that did not evidence the presence of contributions from reactions different from fusion-evaporation, e.g. from preequilibrium emission. A similar behavior has been associated to the population of doorway states [Din16]. However, it has been observed that this phenomenon occurs in α-like nuclei and disappears in similar systems produced with non-like reactants [Apa06]. Therefore this is not the most probable explanation for the observed behaviour.

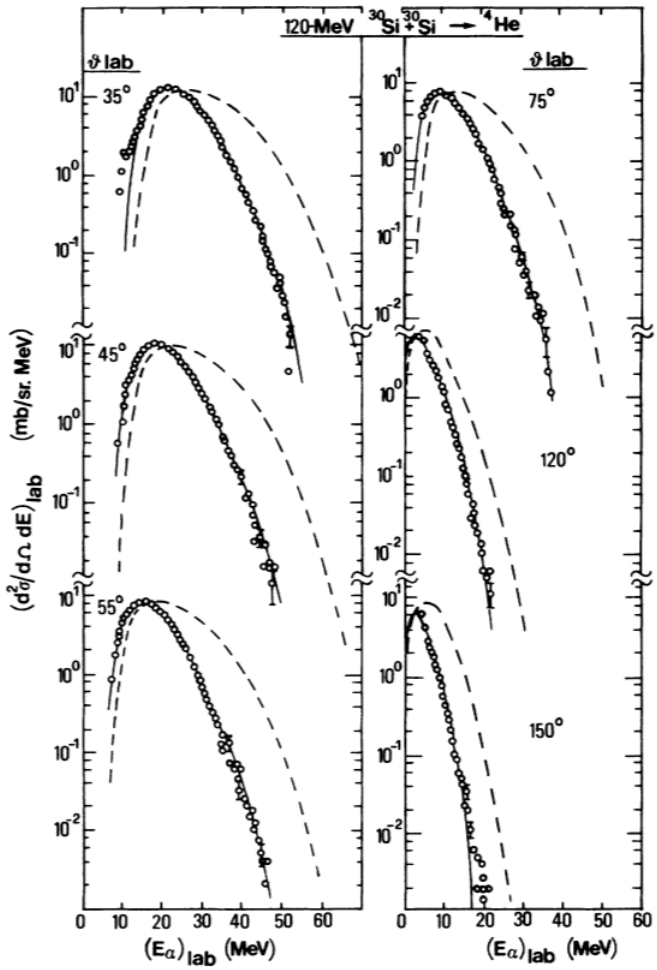

Figure 1.7: α-particle energy spectra at different laboratory angles. The experimental data (dots) are compared with the simulations assuming the emission from spherical nuclei (dashed lines) and from highly deformed nuclei with a $\frac{b}{a}$=3 (solid lines).

The data were investigated by means of comparisons with the SM prediction assuming the evaporative decay from a CN. The possibility to take into account the deformation influence during the multi-step cascade, was not possible at that time due to the lack of a suitable model. Therefore calculations of energy spectra where performed using the computer code GANES, which provides a detailed description

of the coulomb effects on the charged particle trajectories. We have to note that GANES, being a single-step, requires to be combined with multistep evaporative code to define the initial conditions for the emission of the particles when CN at high excitation energies decay through long cascades. Hence, LILITA code was used to calculate the equivalent one step emission conditions at which the particle emissions take place (mean values of mass, excitation energies and angular momentum <A>, <Ex> and <J>).

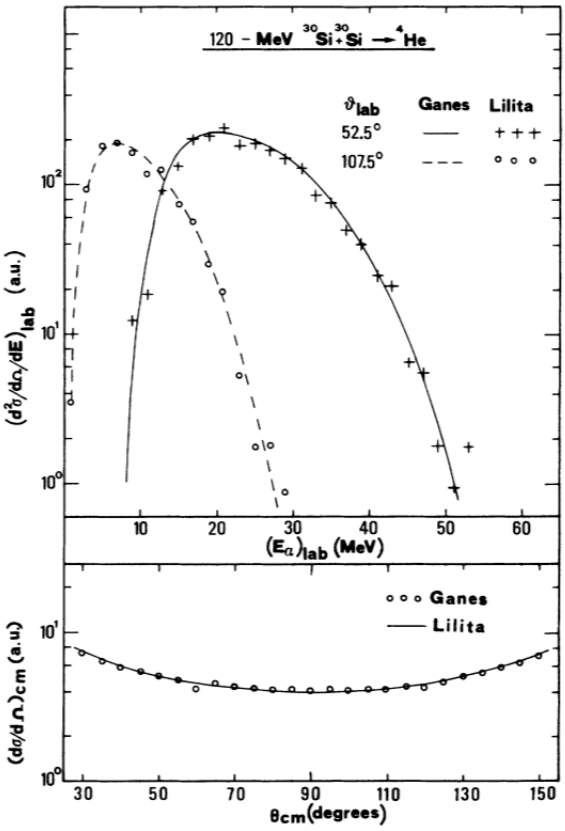

Figure 1.8: α-particle energy spectra at $\theta_{lab} = 52.5°$ and 107.5° and anagular distributions calculated by the code GANES and LILITA assuming a first-step emission.

In order to exclude that the differences between the experimental and simulated

data were depending on the length of the decay cascades, GANES results were validated by means of a comparison with LILITA ones. In Fig. 1.8 the resulting energy spectra and angular distributions are compared. As you can see the distributions obtained with LILITA differ from the GANES ones only if the first step emission is considered, but they are in good agreement if are assumed as initial conditions for the α-particle emission from the equivalent one-step emission. Hence GANES represent a well suited tool for the interpretation of the data able to evidence the presence of deformation effects. On this grounds the authors concluded that the deformation predicted from the RLDM were not sufficient and a new physical model that effectively increase the mean evaporation radius have to be included in the statistical model. We have to note that even if a satisfying description of the energy spectra and angular distributions can be achieved with a single-step model as GANES, more sophisticated multi-step models are needed to provide a realistic description of the whole decay process. In fact, GANES, which does not include the competitions among different evaporation channels (neutrons, protons, alpha-particles, etc.) or different decay processes (evaporation vs. fission), cannot calculate the comprehensive observables as the particle multiplicities or the more exclusive observables such as the particle-particle correlations, which are more sensitive to the evolution of the nuclear shapes along the evaporative cascades. Therefore in order to progress it is essential to consider larger set of observables and to introduce multi-step decay in the codes.

1.3.3 660 MeV ^{60}Ni + ^{100}Mo

Large deformations effects were observed also in studies of heavier systems. The experimental energy spectra of the α-particles, measured in the 660 MeV ^{60}Ni +

^{100}Mo reaction [Gon90] are in fact shifted to lower energies with respect the ones calculated assuming evaporation from a spherical emitters as you can see in Fig.1.9. These effects are typical not only of the α-particles, but exist also in the other He isotopes and in heavier ejectiles, whereas they are absent in the neutron spectra. Hence, this behavior affecting only the charged particle should be connected with the emission from peripheral region where the trajectories are driven by a coulomb potential weaker than the spherical one.

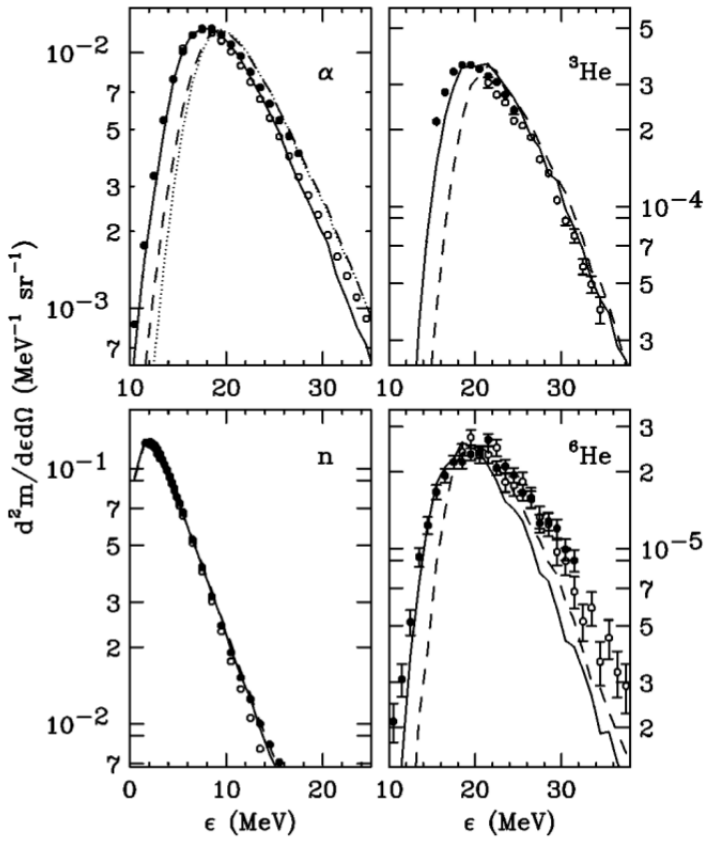

Figure 1.9: α, n, ^{3}He, and ^{6}He energy spectra. The dashed and solid lines indicate the statistical model predictions obtained in simulations with spherical and deformed compound systems, respectively. The dots are the experimental data. The simulations were normalized to the experimental maximum value. The dotted line indicates the particle spectra for spherical compound nuclei (from Ref.[Cha01]).

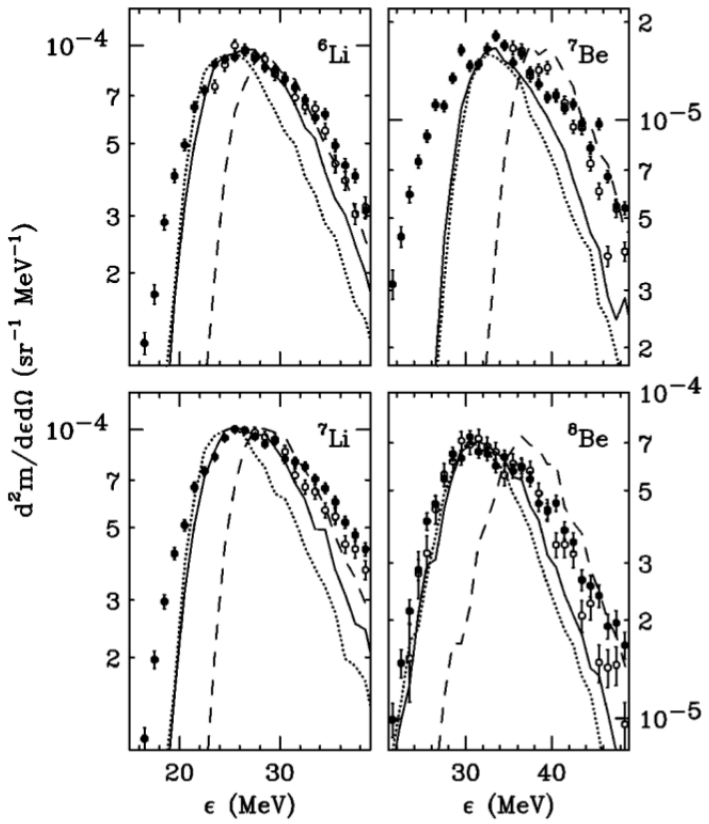

Figure 1.10: Same as Fig.1.9 but for ^{6}Li, ^{7}Li, ^{7}Be, and ^{8}Be ejectiles. The dotted curves are from calculations where the Coulomb barriers were lowered by increasing the radius parameters of the nuclear potentials by a factor 1.25 (from Ref.[Cha01]).

In the work by Charity et al. [Cha01] the experimental data were compared with simulations of the multistep code GEMINI [GEM]. As for the previous system, the calculations give a better reproduction of the shape of the low-energy region by assuming deformations in the compound systems. In this shown calculation, transmission coefficients and rotational energies were assumed appropriate for a fixed prolate deformation with a major to minor axes ratio $\frac{b}{a}$=1.6. At higher excitation energies, the transmission coefficients were obtained by averaging spherical coefficients

over the surface area of the system equivalent sphere approximation [Hui89, Sto81]. Transmission coefficients and rotational energies appropriate for $\frac{b}{a}$=1.25 were set for excitation energies below 100 MeV. This ansatz was chosen because it allows to reproduce the experimental α-particle energy spectrum of ^{164}Yb compound nuclei at $E^* = 101$ MeV measured in Ref.[Cha97]. This approach follows the idea that evaporation is expected to commence before the equilibrium distribution of the shapes is attained. In a such a way the nuclear shapes depend on the entrance channels and larger elongations are expected for more symmetrical reactions in the initial stage. However, measurements of α-particle spectra are in contradiction with this scenario and moreover the simulations do not reproduce the low energy yields for ^{6}Li, ^{7}Li and ^{7}Be ejectiles that require Coulomb-barrier distribution larger than that associated with a single deformation, see Fig.1.10. Therefore, the assumption of a single deformation is too simplistic and a new physics is needed to provide an interpretation of general validity. The differences observed in the energy spectra are directly linked with the deformation of the nucleus at the emission stage. Heavier particles which carry out large amount of energy and angular momenta are mainly emitted at the early stages of the decay cascade, whereas lighter particles, as protons and neutrons, are emitted also in the subsequent steps. Consequently, in order to provide a complete description of the evaporation process it is mandatory to consider particle multiplicities.

In the contest of this thesis, we will consider only protons, neutrons and α-particles, because the heavier particles multiplicities are negligible being orders of magnitude lower.

Table 1.1: Light particles multiplicities for the 60Ni+100Mo reaction compared with the GEMINI predictions [Cha01].

	Mn	Mp	Mα
Exp.	10.2±0.7	4.8±0.8	1.9±0.1
Cal.	8.7	5.3	2.2

Unfortunately, the GEMINI simulations, whose parameters were tuned to well reproduce the neutron and α-particle energy spectra in Fig. 1.9, largely underestimate the neutron multiplicities shown in Table 1.1. Also, this latter discrepancy evidences the inability of the model to provide a reliable description of the evaporation process and the need to look for a missing key physical ingredient. Nuclear deformation alone it is not enough to solve the evident discrepancies.

1.4 Open questions

In the previous paragraphs, spectra, angular distributions and multiplicities of the light particles emitted in the purely evaporative channels, in a sample of reactions from light to medium-heavy compound nuclei, have been shown compared with statistical model predictions. All the predictions, performed by adopting different single-step and multi-step codes, are unable to reproduce the experimental observables all together. The role of multi-step particle emission and competition in the model calculations have been considered and found to be inadequate to explain the observed discrepancies. Furthermore, the discrepancies cannot be attributed to the limitation due to the implementation of the model. In general, different authors evidenced significant change in the behavior of the nuclear matter with increasing of the angular momenta and excitation energies involved with respect to the cold nuclei. The

charged particles energy spectra shapes and angular distributions seem to suggest that large deformations may occur independently from the mass of the compound nuclei and the symmetry/asymmetry in the entrance channels. However, calculations that model statistically deformed nuclear emitters do not give satisfactory overall pictures. In particular, a single set of deformation and reduced barriers does not allow the simultaneous reproduction of the whole set of observables. Therefore, it is crucial to consider large set of observables for a single system in order to avoid controversial conclusions, as for instance in the work of La Rana et al. [Lar87] in which, with a single set of observables, it is possible to reproduce α-particle energy spectra and proton and α-particle multiplicities, but not the proton energy spectra. Although this default of the standard statistical model has been known since decades, at present a solution is still missing even if it is of large importance because the studies of these reaction systems are a benchmark for studies of new frontiers at high energy and spin. Eliminating the effects due deformations and variations of the channel competition at extreme angular momentum, there must be a property of the transition states that increases the radial distance between the emerging charged particles and the residual nucleus. This element could be related to the superficial density, possibility having a tail that is more extended than it is imagined.

In this framework, this Ph.D. research has been devoted to the study of evaporation channels in different region of masses. The main goal was to investigate on possible solutions to the above deficiency of the model at high angular momentum and excitation energies by adopting a non-standard statistical model approach. With this aim the nuclear stratosphere model has been considered because it effectively increases the mean evaporation radius in a manner unattainable by symmetric deformations and allows to achieve a nuclear density distribution depending on the charged particles involved in the evaporation process.

Several technical developments to reduce the computational time for large grid of calculations with the new ingredients in the LILITA standard statistical model have been introduced. The leading parameters for particle emission, e.g. the moment of inertia and the transmission coefficients, have been consistently modified to reach a global description of the emission process (independently for the excitation energies and compound nuclei involved). A systematics analysis for validating the code predictions have been carried out by comparing different data set available in literature. The results obtained seem to provide a better understanding of the decay process. Consequently, model predictions for larger mass system have been performed in order to evaluate the impact of this innovative description on the evaporation process observables for future experimental and theoretical studies.

Chapter 2

Need for a new physics in statistical model

As underlined with many examples in the previous chapter, over many years the statistical model has become the basis for the development of a series of codes dedicated to the simulation of the nuclear evaporation process: neutron and light charged particle energy spectra, multiplicities, cross sections, residue velocities and yield, photon distributions, etc are often computed by using a Monte Carlo approach. However, for some extreme conditions such as high temperature or high angular momentum, the statistical model shows discrepancies with the behavior of the real nuclei, especially as regards the emission of proton and α-particles. Often, the emission barriers appear to be much smaller than the fusion barriers (the reverse process of evaporation according to the detailed balance principle). To compensate for these discrepancies, it is necessary to alter unreasonably the barriers from systematics by changing the emission barriers and the moment of inertia of the compound nuclei. These problems suggest that additional effects are needed in the models.

This PhD work is based on a continuation of the studies so far carried out on the statistical model and the Monte Carlo simulation codes of compound nuclei deexcitation by evaporation of light particles. The main focus is on a possible missing ingredient: the nuclear stratosphere [Lac88]. After the impact of projectile and target in a fusion reaction many particles must be scattered into transitory orbits of very high excitation. The density distribution of this hot composite nuclear system might display a transient stratosphere of "high altitude orbits" that will relax quite rapidly into the density profile of normal Fermi Gas with shape of a rotating liquid drop at equilibrium. A hot very diffuse nuclear surface is therefore formed and promotes evaporative like emission prior to its relaxation. The study of this nuclear stratosphere is carried out on a double path: on one hand, the implementation of this model inside one the existing code on the statistical model; on the other, by improving the computational efficiency of the code and introducing a flexible and easily accessible user interface.

2.1 Nuclear Stratosphere

The statistical model is often in disagreement with the behavior of real nuclei with a temperature of only a few tens of MeV. These differences could lead to underestimating or overestimating some important observables that are essential for the implementation of an experiment. One, above all, is the multiplicity of decay channels: small variations in the model or parameters can significantly change the probabilities of production of a given residual nucleus. This point is for instance of extreme importance in the estimate of the production cross sections of exotic nuclei in different reaction mechanisms (i.e. fission, quasifission, multinucleon transfers) or of superheavy nuclei. Typical discrepancies on measured observables obtained through the

use of the statistical model are shown for instance in Ref. [Lar87] where they have measured both energy spectra and angular correlations of light charged particles. These discrepancies between model and data have been widely observed in different region of mass and excitation energies and for different probes [Gon90][Var10][Din18]. For these reasons this PhD work proposes the implementation of a new physical ingredient in the statistical model. Other similar evidences of the deficiencies of the statistical model are reported in a long series of articles between the late 80s and early 90s.

2.1.1 Nuclear Stratosphere formation at finite temperature

The comparison with the experimental data from many reactions grossly indicates the presence of very low emission barriers, especially for protons, which are typically associated with very large deformations of the emitter. However, such deformations are larger than the predictions of the Rotating Liquid Drop Model. In other words, the nucleus cannot sustain such large predicted deformations. An alternative explanation was proposed by [Lac88] which assumes the presence of a nuclear stratosphere. This concept have been developed in a model by Batko and Civitarese [Bat88].

The theoretical basis for the assumption of a nuclear stratosphere is reported in the Ref.[Boz89]. The observed trends of the energy spectra and angular distributions can be related to the occupation of high lying single-particle levels occurring with the increase of the nuclear temperature and consequent to a change in the distribution of nuclear density. This mechanism is controlled by the thermal response of the mean field and can not be reproduced, for example, by changing the emission barrier or by changing the deformation parameters of the nucleus itself. In Ref.[Boz89] it is proposed to link the density of spatial distribution of nuclear matter as a function

of temperature to the thermal response of the medium to the formation of a nuclear stratosphere. In other words, the increase of the density at the surface region, with increasing temperatures, leads to a decrease of density in the inner region. This transformation determines the formation of a nuclear stratosphere. More generally, at high temperatures, when the nucleus is more excited, a balance between the decrease in the density distribution within and the increase in the density distribution outside should be balanced. This balance is achieved by the contraction of the volume part, which obviously can not contract indefinitely and with the expansion of the part of the surface with the employment of high single-particle orbits.

The increase in the average radius of the surface region, as a function of the nuclear temperature, has as its direct consequence the formation of the stratosphere with the consequent variation of the particle emission probability. If we consider that the radial dependence of the optical model potential is derived from the nuclear distribution function, it becomes clear that the effect of formation of a nuclear stratosphere on the statistical emission of particles must be investigated by incorporating this radial dependence into the standard statistical model. This variation of the density distribution function simultaneously influences different quantities such as the moment of inertia and the transmission coefficients. Therefore a correct evaluation of the global effects requires the implementation of the function in the code so that the overall effect can be assessed on the experimental observables competing with each other. It should be noted that the model thus becomes temperature dependent also in the transmission coefficients because of the dependence of the nuclear radial distribution function on the temperature.

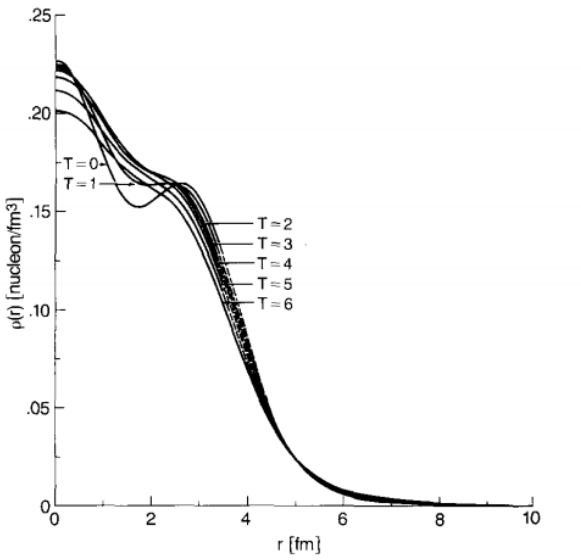

Figure 2.1: Density profiles at various temperatures for ^{56}Ni

In Figure 2.1 are shown the predicted density profile $\rho(r)$ at different temperatures, from 0 to 6 MeV. The model well reproduces the experimental distribution at T=0 of ^{56}Ni where a double hump shape much higher in the inner region is observed. With the increase of temperature these latter differences are smoothed. The structure of light nuclei is well reproduced at zero temperature, and gradually evolves towards systems with a more rounded shape at high temperatures T. Figure 2.2 shows the differences in density for various temperature values as a function of the radial variable r .

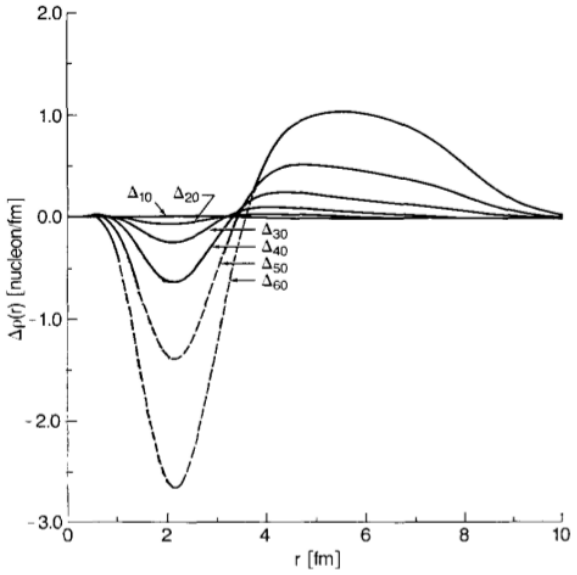

Figure 2.2: Density variation correspond to ^{56}Ni

The evolution of the surface density determines the formation of the nuclear stratosphere. In all cases, however, the internal region can be represented by a Gaussian with a center near the root of the mean quadratic radius and this is the starting point for the modeling of this phenomenon.

2.1.2 Radial dependence of potential

In order to introduce this element into the statistical model, the following approximations of the radial dependence of the central potential were then used for the calculation of the transmission coefficients: contracted Woods-Saxon plus a surface centered Gaussian (CSWG) and a contracted Woods-Saxon plus a tail at the surface region (CWST). The function obtained is then replaced within the optical potential that we remember to be defined as:

$$V(r) = -V_o f_v(x_v) + (\frac{\hbar}{mc})^2 V_{SO}(s \cdot l)\frac{1}{l}\frac{d}{dr}[f_{SO}(x_{SO})] \tag{2.1}$$

$$W(r) = -W_v f_w(x_w) + 4W_s \frac{d}{dx_s}[f_s(x_s)]$$

where $f_i(x_i) = \frac{1}{(1+e^{x_i})}$ with $x_i = \frac{(r-R_i)}{a_i}$. In the case of CWSG approximation, the function is:

$$f_i^{CWSG}(x_i) = f_i(x_i + 1) + h^{CWSG} e^{[-(x_i-1)^2]}$$

both for the volume part V_v and W_V of real and imaginary potential. Since the presence of the stratosphere also changes the charge distribution within the nucleus, the Coulomb potential must be adapted appropriately. In the uniform charge approximation of the Coulomb potential given as :

$$V_C(r) = \begin{cases} Z_1 Z_2 \frac{e^2}{r} & (r \geq R_c) \\ Z_1 Z_2 \frac{e^2}{2R_c(3-\frac{r^2}{R_c^2})} & (r \leq R_c) \end{cases} \tag{2.2}$$

the radius R_C is replaced by R_c^{CSWG} given by $R_C - a_v$, consistent with a contraction of the volume region of the density distribution function as described in the previous section. With this approximation of the radial dependence of the potential we can describe the behavior by which, at the finite temperature, the radial density distribution function is concentrated in its volume region and shows a cluster localization in the surface region. Despite the good approximation achievable with CWSG potential is preferable to use the CWST approximation.

The CWST is defined by the following radial dependence:

$$f_i^{CWST}(x_i) = \begin{cases} \frac{1}{(1+e^{x_i})} & r \leq r_i^M \\ h & 0 \leq r - r_i^M \leq b \\ 0 & r \geq r_i^M + b \end{cases}$$

where $x_i = (r - 0.8R_i)/a$ and $r_i^M = 0.8R_i + a_i ln[\frac{(1-h)}{h}]$ for the part of both real and imaginary volume of the optical potential. Within the same approximation we define the Coulomb radius as $R_c^{CWST} = 0.8R_C$.

We must remark that all the approximations proposed do not have explicit dependence on the temperature, but the tuning of the parameters b and h, related with the density function, can be used to probe their dependence on the temperature, namely the excitation energy of the compound nucleus. The dependence of b and h on the temperature has a direct effect on the transmission coefficients because of the radical change of the optical model potential. Therefore, in the following tests of the statistical model, with the inclusion of the stratosphere concept, we will try to find empirical relations of the type $b(T)$ and $h(T)$ from the best values of b and h which reproduce the available set of data for a given compound system at a given temperature. The identification of such a relation would give the first evidence of the existence of this stratosphere effect and would give further positive impact to the use of this model as a broad predictive tool.

2.2 Parameterization of the optical potential

To use the potentials described above within the statistical model we have used the following parametrizations: the one developed in 2003 by Koening and Delaroche [Kon03], valid for neutrons and protons, and that was developed from valid for α-

particles. Unlike other works in which local parametrizations valid for certain energy and mass regions have been determined, the main work of Koning and Delaroche was based on defining a *global* potential that reproduces the observed data in a wide range of nuclides and energies. In fact, it is known that there are large differences in behavior between stable and exotic nuclei. In order to try to include both types of nuclei, in the parameterization of the global potential, the authors introduce a dependence on isospin through the term $\frac{N-Z}{A}$. In this way, the effects due to the distance from the valley of stability are taken into account. Also in the case of α-particles the work of Xin-Wu Su in 2015 [Xin15] improves the α-particle optical model potential in the range $20 \leq A \leq 209$. The use, for all three particles, of a global potential for the calculation of the transmission coefficients allows us to comfortably extend the statistical model predictions also in areas far from the valley of stability.

2.2.1 Protons and Neutrons

For neutrons, Koning's study was based on 800 angular distributions of elastic diusion $\mathrm{d}\sigma\ \mathrm{d}\Omega$ and 140 sets of cross sections. The systematic takes into account nuclides with $24 \leq A \leq 148$ e $194 \leq A \leq 209$. Nuclides outside these ranges are either too light or too deformed. The difference observed is, for energies above 5 MeV, of 1% and never more than 2%. It can be noted that the analysis is brought to energies equal to 250 MeV but here the Optical Model deviates from the data in a meaningful way; therefore, we set the maximum limit of this parameterization at 200 MeV. For the protons, however, the study was based on 250 angular distributions of elastic diffusion $\frac{\sigma(\theta)}{\sigma Ruth}$ and a large collection of reaction cross sections σR. However, the obtained fits for the proton data are of lower quality compared to those relating to

neutron diffusion, due effect, both at the inefficiency of the angle $\frac{\sigma(\theta)}{\sigma Ruth}$ at higher energies of 150 MeV than at the loss of validity of the Saxon-Wood form factor. Nevertheless, the difference between calculated and measured reaction cross sections varies between 5% and 10%, so that the parameterization is still satisfactory.

2.2.2 α-particles

For α-particles we use a recent set of global phenomenological optical model potential parameters obtained by simultaneously fitting the experimental data of reaction cross-sections and elastic scattering angular distributions in the mass range of target nuclei $20 \leq A \leq 209$ at incident energies below 386 MeV [Xin15]. This set of parameters reproduces satisfactorily the total reaction cross sections and elastic scattering angular distributions, in a very wide region including nuclei not very close to the valley of stability. Therefore it is more suited to make predictions in the region of more exotic nuclei, with respect to the local parametrization usally adopted [Hod84]. The use of a global potential has the great advantage of not having to be changed at every simulation carried out by reducing the number of variables between the different simulations considered.

2.3 Nuclear Stratosphere for a light nucleus

In order to evaluate the impact of the nuclear stratosphere model and the new transmission coefficients on the typical observables of the evaporative decay of the CN, we have run the following calculations with the statistical model code LILITA. In the first phase, the compound nucleus $^{67}Ga^{*}$, produced by the reaction 190MeV ^{40}Ar + ^{27}Al, was taken into consideration. The used code employs the transmission co-

efficients calculated using, for protons and neutrons, the optical potential through the parameterization of Koning [Kon03] while for the α-particles that of Xin [Xin15]. The scope is to compare calculated observables such as energy spectra, angular distributions and multiplicity for different parameters of the radial function given by the classical Saxon Wood and the CSWG defined in the last section. In view of the considerations reported in the article [Bat88] we expect to obtain different values of the observables in the two cases. We will then use the knowledge acquired from this comparison to investigate reactions in extreme conditions.

2.3.1 Energy distributions

The first observables we considered are the energy spectra produced by the decay of ^{67}Ga* at excitation energy of 91 MeV and $J_{ER} = 46\ \hbar$. The energy spectra were calculated by adopting different descriptions of the nuclear density, namely, 1) the radial function introduced by Batko and Civitarese [Bat88] for the nuclear stratosphere with different values of b and h and 2) that obtained using the classical Saxon Wood radial function so far indicated as No-Stratosphere(NS). The calculations have been performed by considering the $b = 1$ and 3 fm and $h = 0.05$ and 0.15 in order to evidence the influence of these parameters on the observables of interest. In the Fig.2.3 are shown the energy spectra in the CM with and $b = 1\ fm$, 3 fm and the simulation NS.

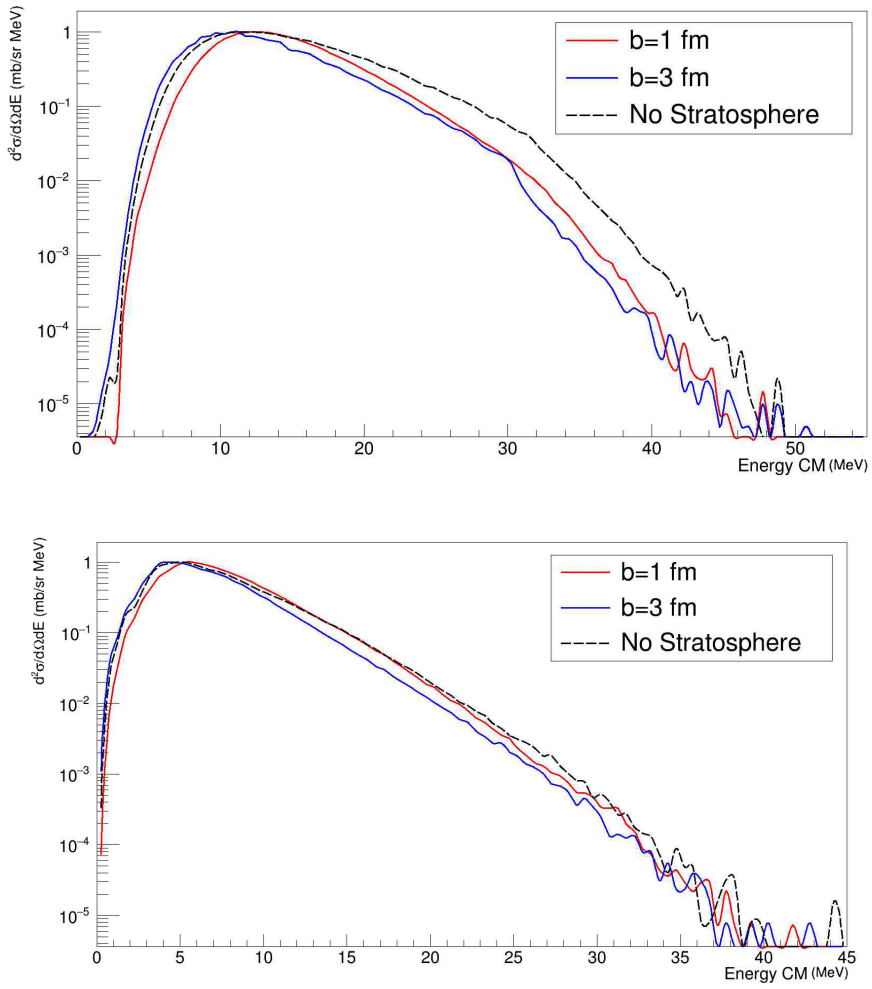

Figure 2.3: α-particles (top) and proton(bottom) energy spectra calculated by the LILITA_N18 code for $^{67}Ga^{*}$ using the nuclear density distribution NS and the nuclear stratosphere with $h = 0.05$ and $b = 1\ fm$ and $3\ fm$.

By comparing the simulated spectra we observe a steeper slope in the higher energy side when we introduce a distribution of the density according to the nuclear stratosphere. The effect is a shift of the position of the maxima at higher or lower energies depending on the specific b and h values, as you can see in Fig.2.3 and 2.4.

The use of a larges extension of the stratoshpere distribution ($b = 3\ fm$) produces a shift of the spectra to lower energies and a steeper slope of the high energy side of the α-spectra, whereas the high energy side of proton is the same. In 2.4 we show the energies spectra produced by fixing the extension of the nuclear stratoshpere at $b = 3\ fm$ for different values of h. The main effect is a shift of the maximum of the $\alpha-$particles to higher energies increasing h and a swelled slope. Simultaneously protons show a diametrically opposite behavior.

It is important to remark that the change in the transmission coefficients introduced with the stratosphere model has an impact on the competition between particle emission probabilities at the different step of the evaporative cascade. Using this stratosphere model the higher density in the most peripheral regions, given the high value of h, modifies the competition among the proton and alpha emission, disfavoring the evaporation of the α-particles and favoring proton emission, whereas the increase of the extension, given by b, leads to the lowering of emission barriers and the increase in low-energy emissions. Therefore, the nuclear stratosphere model introduces a large variability in the energy distributions of the evaporated protons and α-particles. This feature is important for the case of $^{67}\mathrm{Ga}^{*}$ as will be shown later.

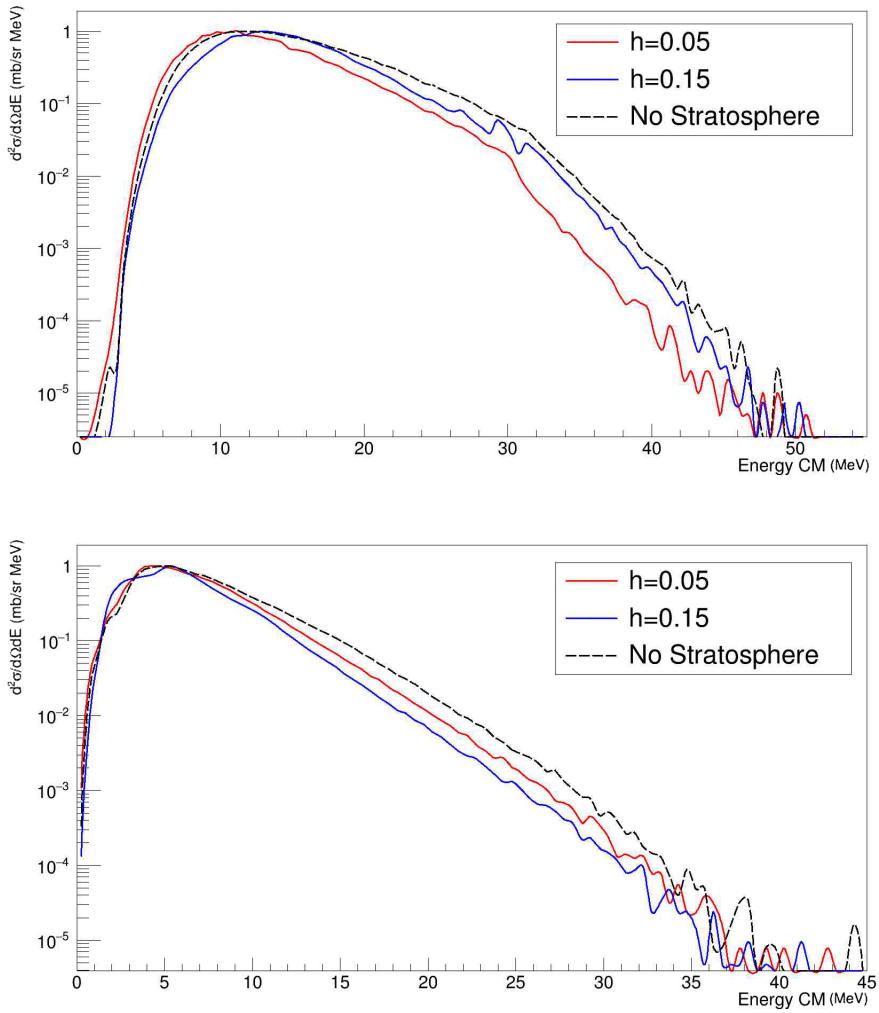

Figure 2.4: As Fig.2.3, using the NS and nuclear stratosphere with $b = 3\ fm$ and $h = 0.05$ and $h = 0.15$

2.3.2 Angular Distribution of emitted particles

Like the energy distributions, the angular distributions in Ref. [Lar87] also showed a marked difference from those calculated using the statistical model. We begin, as in the previous section, to examine the angular distribution in the center of mass

keeping $h = 0.05$ and varying b.

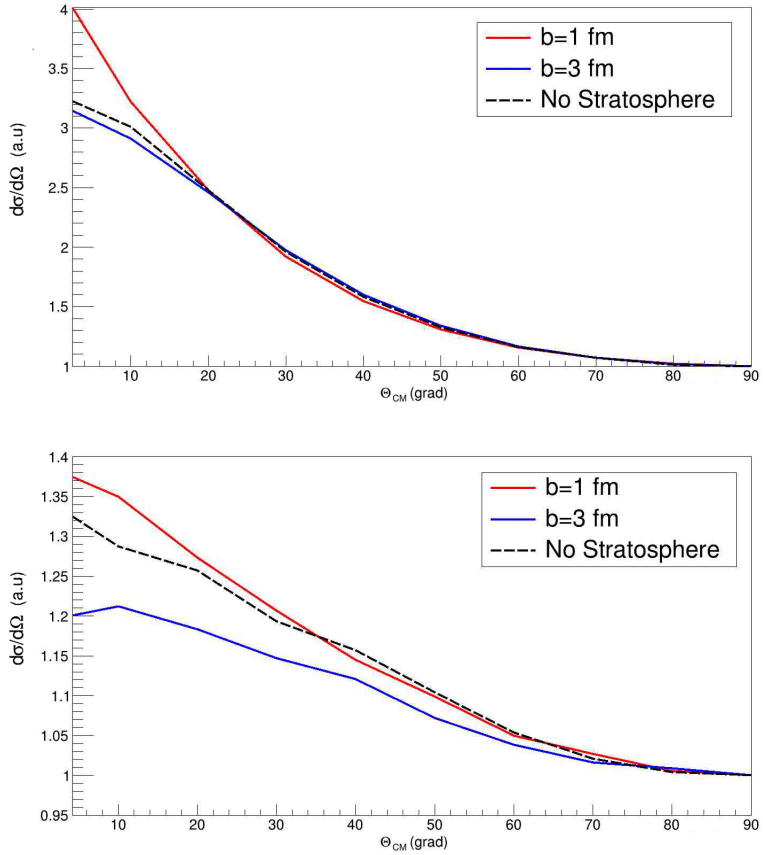

Figure 2.5: α-particles (top) and proton(bottom) angular distribution in CM spectra calculated by the LILITA_N18 code using the nuclear density distribution of (NS) and the nuclear stratosphere with h = 0.05 and b = 1 fm and 3 fm .

In general, by observing Figg.2.5, 2.6, 2.7 and 2.8 the introduction of the stratosphere produces angular distributions that tend to be more anisotropic in the case of α-particles while more isostropic in the case of protons than the distribution generated by the model without the stratosphere.

Higher values of b for both protons and α-particles produce more and more

isotropic distributions. This trend is certainly due to the fact that a growing b parameter increases the spatial extension of the density distribution, with a consequential increase of the moment of inertia of the nucleus. Hence, the angular distribution tends to become more isotropic. This effect, more evident in the case of protons, is mitigated as h increases as can be seen in Fig. 2.6

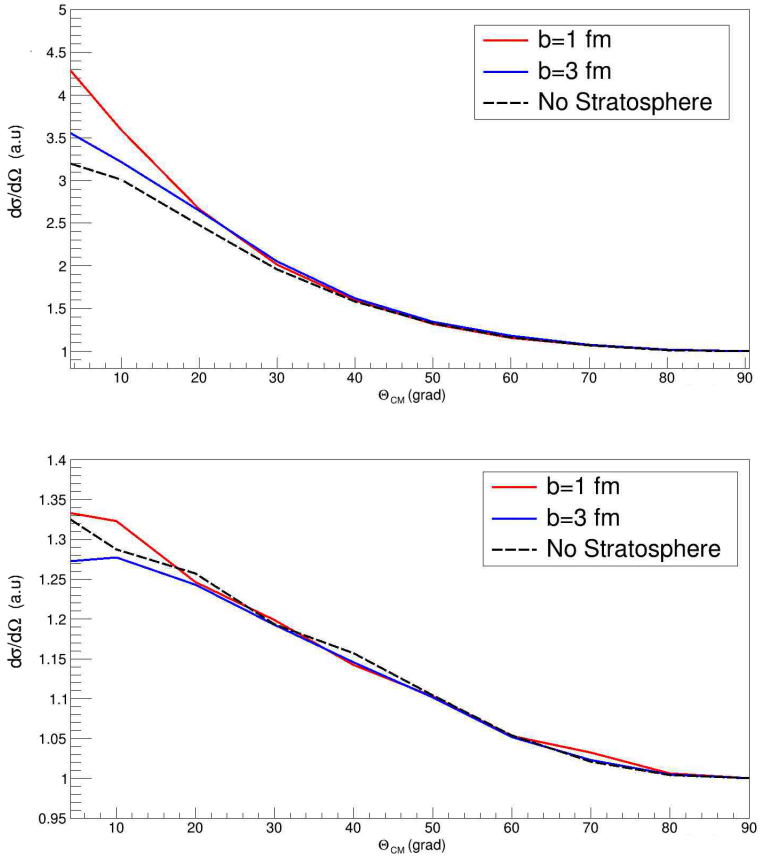

Figure 2.6: As Fig.2.5 Angular distribution of α-particles(top) and protons(bottom) emitted with $h = 0.15$

In Figs.2.7 and 2.8 the angular distributions are computed for $b = 1\ fm$ and two values of h. In this case, the trend is the opposite of the one found by increasing b:

the isotropy is reduced by increasing the h values. In other words, the anisotropy increases with h and decreases with b.

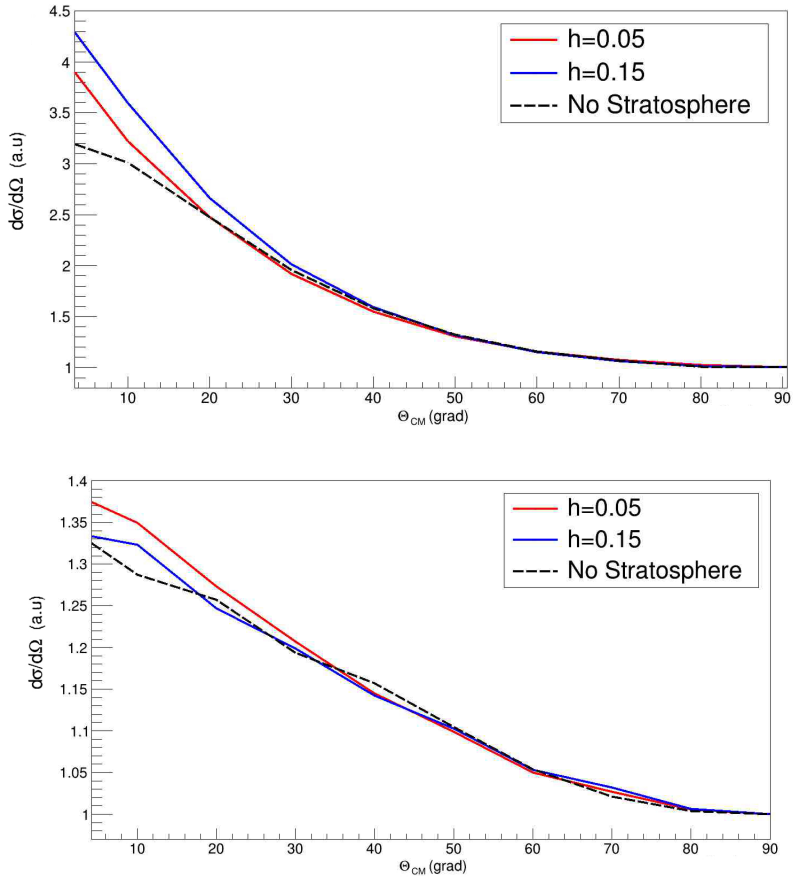

Figure 2.7: Angular distribution of α-particles(top) and protons(bottom) emitted with $b = 1\ fm$

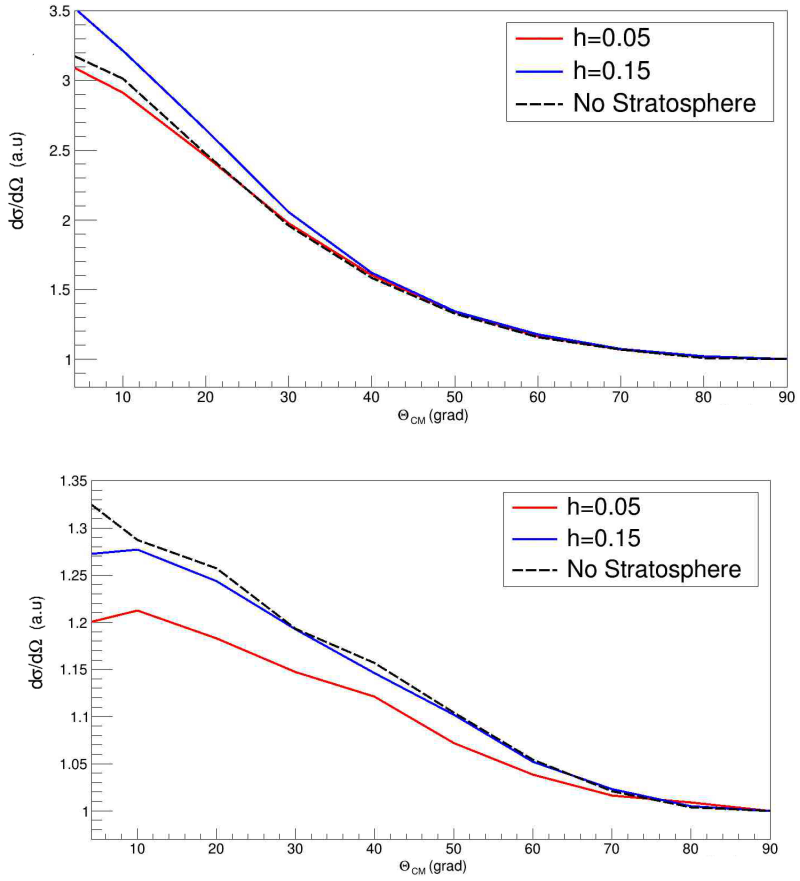

Figure 2.8: Angular distribution of α-particles(top) and protons(bottom) emitted with $b = 3\ fm$

2.3.3 Multiplicity of decay channels

The multiplicities of the emitted particles (average number of particles of one type per decay chain) are very sensitive observables to probe the statistical models because they include the competition between the different decay channels, which in turn depends on each particle emission probability computed by mixing transmission coefficients and level density. Therefore, the multiplicity values are closely connected

both with the angular momentum and the excitation energy of the compound nucleus. The study of these observables becomes even more effective when different light particles, i.e. protons, neutrons, and α-particles, are emitted in sufficient amount to be simultaneously measurable. For this reason, as it will be shown later, the comparison with the data measured in the reaction 660 MeV ^{60}Ni + ^{100}Mo [Cha01] represents an important test bench for assessing the impact of the transmission coefficients introduced from stratosphere model.

The competition between different evaporation channels gives rise to a distribution the evaporation residues. Therefore, a possible way to test the calculation of the particle multiplicities is to compare the calculated evaporation residues distribution with the measure one if any. Tabs. 2.1 and 2.2 show the production cross section of evaporation residues from ^{67}Ga* for different values of h and b. In the lack of any previous knowledge on the effect of changes in the values of h and b on the evaporation residues distribution, we performed a grid of calculations with the hope of finding a pattern that allows to unambiguously define the behavior of the production cross sections with varying h and b.

Produced Nucleus	Cross section(mb)			
	h=0.05	h=0.1	h=0.15	NS
N=31 Z=28	164	164	164	117
N=30 Z=27	152	152	129	152
N=32 Z=28	105	105	117	47
N=30 Z=26	82	82	70	141
N=33 Z=29	70	70	58	35

Table 2.1: Cross sections of the main nuclei produced by ^{67}Ga* and calculated with $b = 1\ fm$.

Produced Nucleus	Cross section(mb)			
	$b = 1\ fm$	$b = 2\ fm$	$b = 3\ fm$	NS
N=31 Z=28	164	82	58	117
N=30 Z=27	152	129	70	152
N=32 Z=28	105	35	23	47
N=30 Z=26	82	129	141	141
N=33 Z=29	70	82	129	35

Table 2.2: Cross sections of the main nuclei produced by ^{67}Ga* and calculated with $h = 0.05$.

For b = 1 fm (Tab. 2.1), we do not appreciate significant variations in the production cross section for different values of h. On the contrary, if h = 0.05 (Tab. 2.2), the variation b induces important alterations. However a clear pattern does not come out from these calculations as a function of h and / or b. Considering the scarcity of data available (due to the high complexity required by the measurement of the evaporation residues cross sections) it is more useful now to switch the calculations to the particle multiplicities.

The calculated multiplicity of light particles from ^{67}Ga* are shown in Fig. 2.9 for the different models.

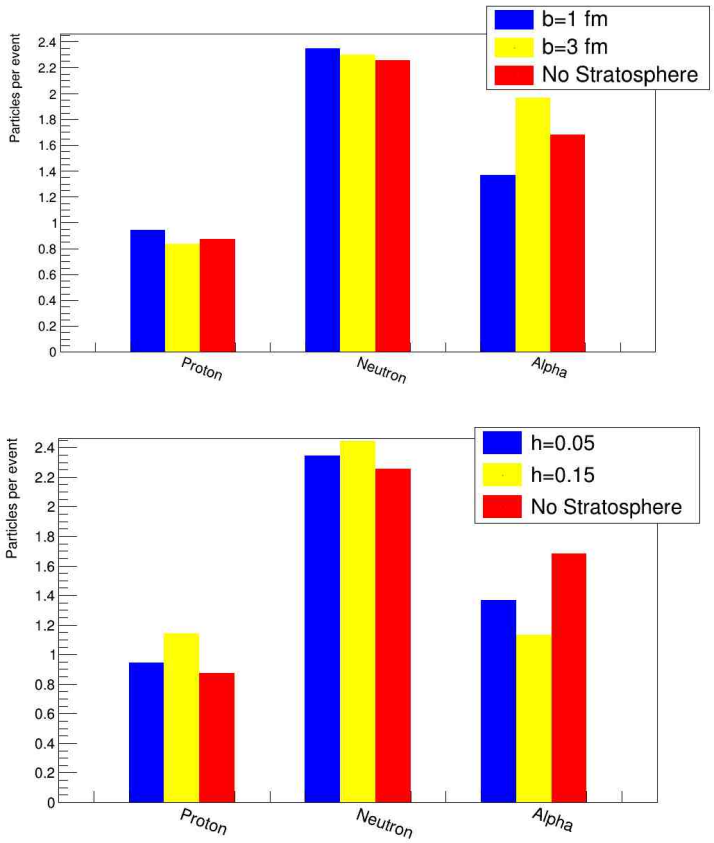

Figure 2.9: Particles emitted per event with fixed $h = 0.05$(top) e $b = 1\ fm$(bottom)

The calculations indicate that proton and neutron multiplicities decrease as b increases while they grow with h. Thus, the α-particles increase consistently in the passage from $b = 1\ fm$ to $b = 3\ fm$ and decrease as h increases. With lower values of h it seems therefore that a greater extension b of the stratosphere favors the emission of α-particles at the expense of neutrons and protons.

A higher density and greater extension of the stratosphere shows a similar trend to the previous one, as shown in Tabs. 2.4 and 2.3 for the production cross sections of the evaporation residues.

Produced Nucleus	Cross section(mb)			
	b=1 fm	b=2 fm	b=3 fm	NS
N=31 Z=28	164	164	117	117
N=30 Z=27	152	129	94	152
N=32 Z=28	117	105	59	141
N=30 Z=26	47	59	94	59

Table 2.3: Multiplicity of some of the most populated emission channels with $h = 0.15$

Produced Nucleus	Cross section(mb)			
	h=0.05	h=0.1	h=0.15	NS
N=31 Z=28	59	105	117	117
N=30 Z=27	152	117	94	152
N=32 Z=28	141	141	141	141
N=30 Z=26	59	82	94	59

Table 2.4: Multiplicity of some of the most populated emission channels with $b = 3\ fm$

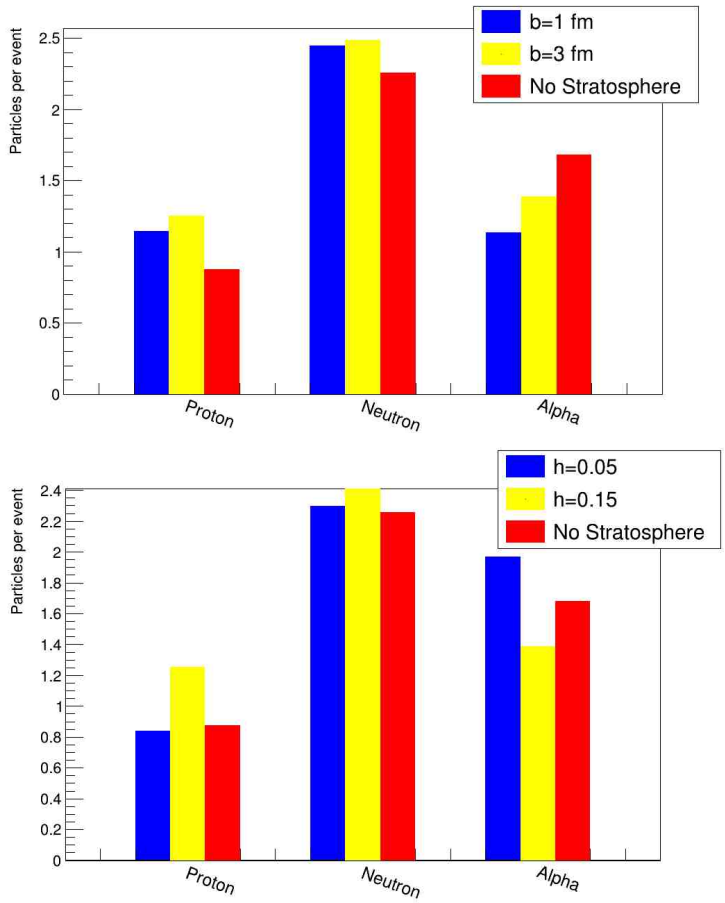

Figure 2.10: Particles emitted by event with $h = 0.15$ (top) and $b = 3\ fm$ (bottom)

In Fig. 2.10 we see that higher value of ^{67}Ga*, combined with a strong extension of the stratosphere b=3 fm, increases the probability of proton emission at the expense of α-particles. The number of neutrons emitted remains, however, almost unchanged. From the overall multiplicities pattern it is clear that the increase in the extent of the stratosphere reduces the number of protons emitted, conversely it grows with h.

2.4 Nuclear Stratosphere for heavy Nuclei

Once the variations induced by the use of the nuclear stratosphere model on the de-excitation of a light compound nucleus have been analyzed, it is essential to evaluate the validity of the stratosphere model in the region of heavier mass nuclei. The reaction considered for this purpose is 340 MeV ^{84}Kr + ^{116}Cd $\rightarrow$ ^{200}Po* with excitation energy equal to 43 MeV and J_{ER}=52$\hbar$ [Han87].

In Fig. 2.11 the energy spectra of the α-particles present, albeit to a lesser extent, a shift towards lower energies. For protons we observe an increase of the particles emitted in the central region of the distribution with slight involvement of the regions of tail and climb. The energy spectra therefore exhibit the same behavior as the energy spectra obtained by simulating the decay of a light nucleus. However the variations induced by b and h are more evident in the high-energy region while less appreciable in the rising region of the distribution.

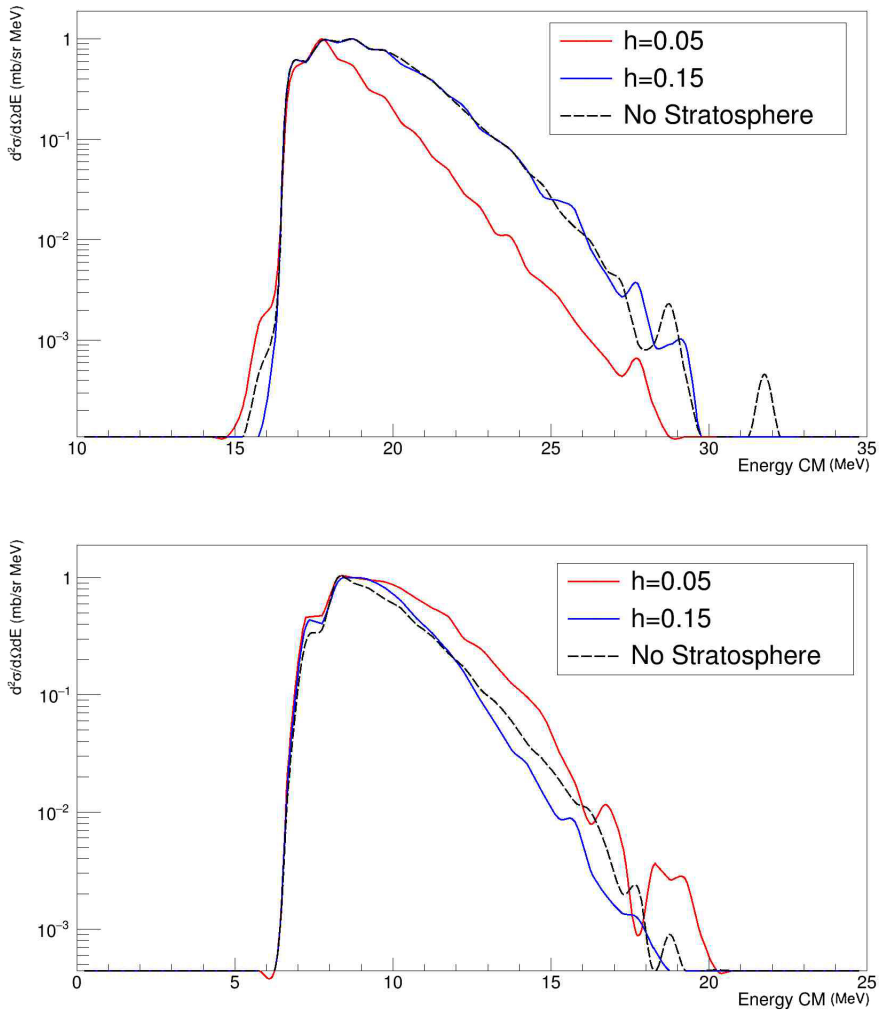

Figure 2.11: α-particles(top) and proton(bottom) energy spectra calculated by the LILITA_N18 code using the nuclear density distribution of (NS) and the nuclear stratosphere with $b = 3\ fm$ varing h.

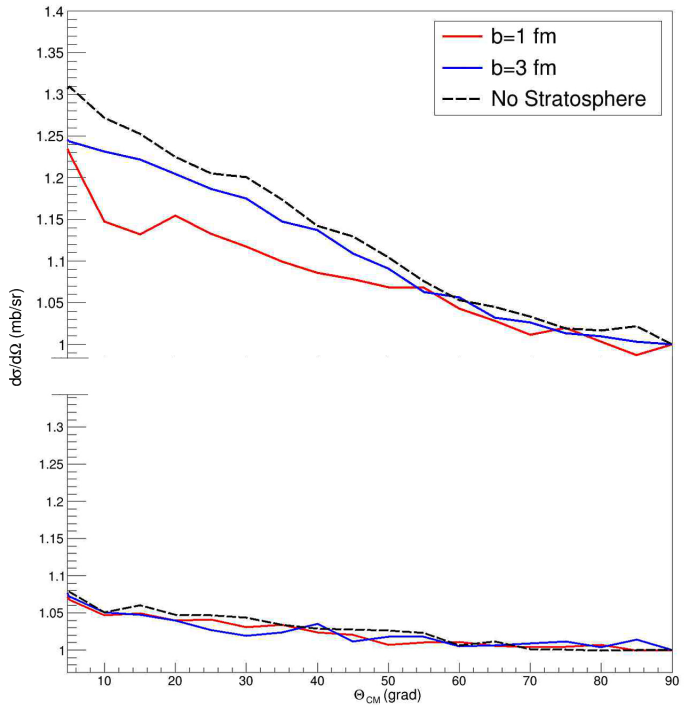

Figure 2.12: Angular distribution of α-particles(top) and proton (bottom) emitted with $h = 0.05$

Angular distributions in Fig. 2.12 show a slightly different behavior from that identified in simulations concerning light nuclei. For α-particle, increasing b corresponds to an increase in anisotropy. In Fig.2.13, on the contrary, for higher value of h the behavior is that found in the case of the light nucleus but the tendency toward higher anistropy in this case is mitigated by the larger moment of inertia.

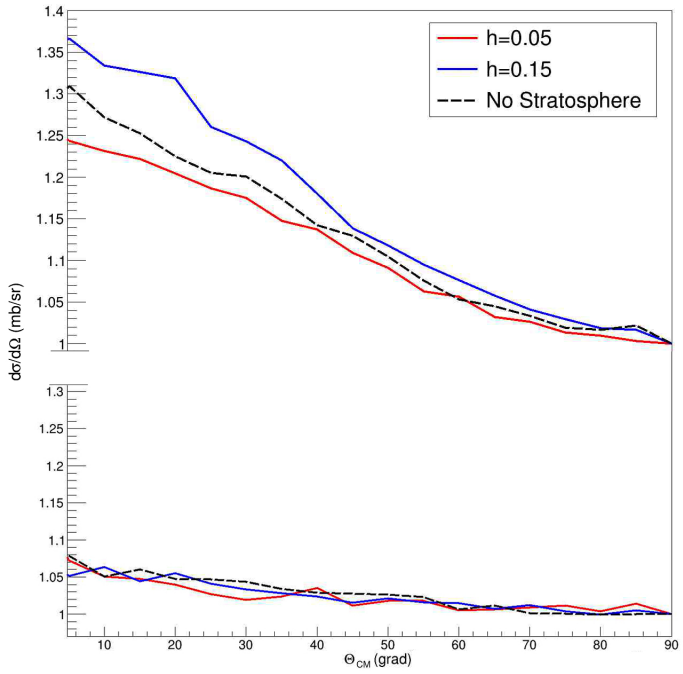

Figure 2.13: Angular distribution of α-particles(top) and proton (bottom) emitted with $b = 3\ fm$

As it concerns for the angular distribution of protons, the Figs. 2.12 e Fig.2.13 reiterate the behavior already observed in the emission of protons with an almost flat distribution. No difference is observed between the three simulations carried out, however we can underline a slight increase of anisotropy that we find for the combination $b = 3$ and h =0.15 in Fig.2.14.

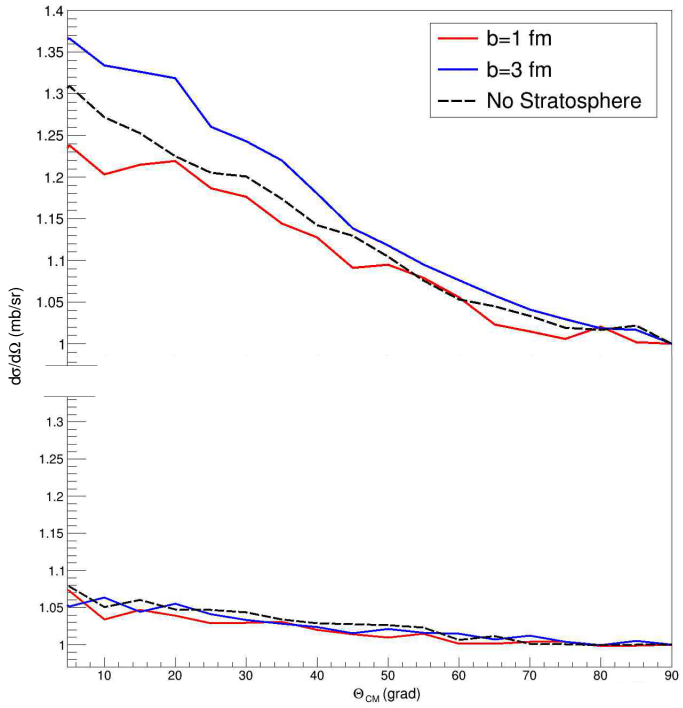

Figure 2.14: Angular distribution of α-particles(top) and proton (bottom) emitted with $b = 3\ fm$

In Figs.2.15 and 2.16 the multiplicities of the evaporated particles are reported. In the comparison between the multiplicities obtained through the use of the model with statosphere and without, the number of neutrons emitted is always slightly higher in the presence of the stratosphere independently of the parameters used, whereas the variations on charged particles are strongly dependent on the parameters: the increase of b leads to the increase in the number of charged particles, instead the increase in density favors the emission of protons at the expense of the $\alpha-$particles.

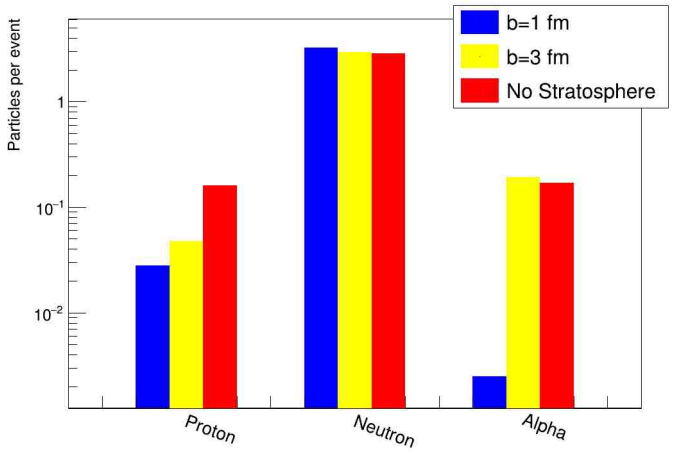

Figure 2.15: Multiplicity using $h = 0.05$

In the case of high density in the outer region ($h = 0.15$) the increase of b produces a lowering of the emission barriers both for protons and for α-particles, with an increase of multiplicity more evident for the protons than for the α-particles with respect to the case of low density ($h = 0.05$), cf. Figg.2.15 and 2.16.

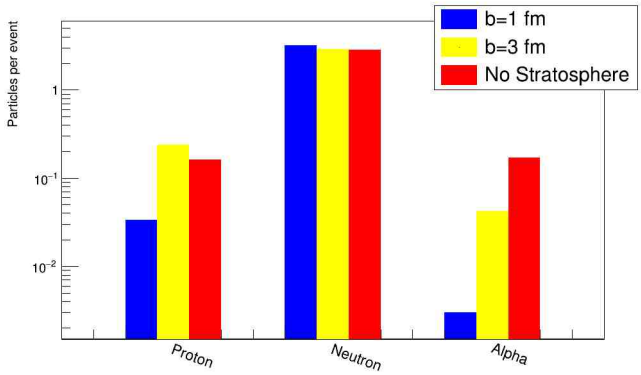

Figure 2.16: Multiplicity using $h = 0.15$

2.5 Final considerations on the calculated trends

We introduced this chapter by hypothesizing the possibility that the use of a stratosphere model would have filled the differences, highlighted in a series of publications, between the measured and the calculated physical observables using the standard statistical model.

Regarding the multiplicity of evaporated particles, the introduction of the stratosphere model, both for light and heavy systems, produces similar results. In both cases variations in density and extension of the stratosphere mainly influence the multiplicity of protons and α-particles; the increase of the density, for example, favors the emission of protons while the increase of the extension of the stratosphere favors the emission of the α-particles. A heavy system is, however, more sensitive to variations than the light one. Such behavior could, in fact, explain the differences found in Ref. [Cha01] between calculated and measured multiplicities.

Regarding the angular distributions, the heavy system is less exposed to the variations introduced by the stratosphere. This is because they are probably mitigated by the contribution of the moment of inertia of the nucleus under examination. For the light nucleus, on the other hand, the differences between the measured and calculated angular distributions recall those highlighted in Ref. [Lar88] in support of the thesis that the differences are due to the presence of an increase in the nuclear radius. Instead, the energy distributions of the light evaporated particles show, both for light and heavy systems, significant variations; the presence of the stratosphere, in fact, introduces important shift of the distribution or variations of its shape.

In summary, all the differences among the simulated observables, induced by the use of the stratosphere model, are compatible with those highlighted in the Refs. [Lar88, Cha01, Lar87]. We, therefore, continue in the next chapter with the use the

stratosphere model just explored to reproduce the systems described at the beginning of this chapter with particular attention to the measured observables that present a gap with those obtained through the use of the Standard Statistical Model.

Chapter 3

Using Nuclear Stratosphere Model

As showed in the first chapter, the standard SM does not provide a global description of the evaporation process. Especially, it does not allow to predict precisely the observables produced in the decay of compound nuclei at high angular momenta and high excitation energies. The typical approach adopted so far has been to provide an interpretation of the single experimental data set through the introduction of very large deformed shapes, *ad hoc* modifications of the emission barriers and level density parameters. However, these modifications do not provide a simultaneous and satisfying reproduction of all the observables and do not represent a solid basis for reliable predictions. Above all, by reviewing the literature, these modifications do not bring out a pathway to follow to improve our knowledge of the evaporative decay. Therefore, the need of new physics has been claimed.

In this framework, the aim of the present work is to make a step forward in the understanding of these aspects, whose explanation is still missing. Therefore, at first, we identify a series of experimental data set of fusion-evaporation reactions at extreme conditions for the validity of the SM. The reactions considered are dis-

tributed over a wide nuclear mass range (A=60-160) with large differences in the entrance channel asymmetries and/or the formation of doorway states. Therefore, the inability in the data reproduction cannot be attributed to a specific mechanism as in the case of alpha-clustering nuclei [Din16, Apa16], but they are most probably due to the decay process itself. In order to provide a most general approach, the same parametrization has been adopted for all the leading ingredients of the new version of the evaporative code LILITA as it will be shown in details.

For the above reasons, a new physical ingredient, the nuclear stratosphere, and non-local transmission coefficients have been introduced. In particular, the nuclear stratosphere provides a description of the nuclear matter distributions valid for an extended mass range and does not require modifications depending form the analyzed observables; while the global transmission coefficients for protons and neutrons [Koe03] and α-particles [Xin15] are valid for a mass range of A=20-209 and an energy range covering of several orders of magnitude (1 keV-200 MeV). In a such way it is possible to manage consistently the main aspects concerning the decay processes occurring in a large variety of excited nuclei and the emission competition of the different light particles is treated consistently. In order to validate our approach and to provide indications of the predicting power of the upgraded code we compared the simulations with the exclusive observables collected in different experiments.

In this chapter we present the analysis of the highly excited systems ^{60}Ni, ^{67}Ga,^{160}Yb, produced at Ex=75-93-280 MeV by the reactions ^{30}Si + ^{30}Si, ^{40}Ar + ^{27}Al, ^{60}Ni + ^{100}100Mo, respectively. The three analyses have been performed using a grid of calculations, keeping a= $\frac{A}{8.0}$ costant and changing the two parameters of nuclear stratosphere h and b only, in order to obtain the better reproduction of the whole experimental data set. At the end of this chapter, in order to evaluate the predictive power of the newer code with parameters b and h whose trend, with the excitation

energy or temperature, is derived from the analysis on the above known reactions, predictions for a heavier nucleus have been discusses in terms of changing of evaporation residues yields and multiplicities with h and b from the trends determined from the analyzed systems.

3.1 190 MeV ^{40}Ar + ^{27}Al

The first reaction analyzed within the framework of the new LILITA code is 190 MeV $^{40}Ar + ^{27}Al$, forming the compound nucleus $^{67}Ga^*$ with excitation energy of 91 MeV and $J_{ER} = 46\ \hbar$. As reported in Ref.[Lar87], and discussed in the first chapter, the standard statistical model fails to reproduce both the proton and $\alpha-$particle energy spectra as well as the angular distributions. The authors attempted to reproduce the experimental data by assuming very large deformations. However, a single combination of parameters does not provide a satisfying reproduction of the full set of observables.

In order to verify if the discrepancies observed can be attributed to the use of parametrization valid only on a reduced interval of mass and excitation energy ranges, as a first step, we performed a series of calculations with the standard statistical model in which parametrizations based on a wider systematics have been implemented. As it will be shown in the next section, some improvements have been noticed. However, the main discrepancies still persist and motivate the use of the nuclear stratosphere model.

3.1.1 Analysis based on simulations with Standard Statistical Model

In this section we compare the data with the calculations performed considering the standard statistical model (SSM) implemented in the code LILITA with the new parametrization for the transmission coefficients. In Fig. 3.1 the proton and α-particles energy spectra are shown.

The proton energy spectra are quite well reproduced as well as the low-energy side of α-particles spectra. Discrepancies on the high-energy side of the α-particles energy spectra still exist. The simulated energy spectra of α-particles show a less steeper slope, which can indicate both an overestimation of the Coulomb force at emission stage or a smaller nuclear temperature. However, the simultaneous reproduction of the proton spectra seems to exclude the latter and indicates the deformation as the most probable reason.

The consistent improvement in the reproduction of both energy spectra with respect to the Statistical Model calculations reported in Ref.[Lar87] (see Fig.1.5) has to be attributed both to the use of a multistep code and the new TCs. It is well known that the TCs are very effective on the low-energy side of the energy spectra. Consequently, we can conclude that the parametrizations adopted in the new code are much better suited for the reaction under analysis. We can expect a general improvement also for other systems because we have used a global parametrization instead of a local one of previous analyses. At the same time, the good reproduction of the full proton spectrum indicates an improvement in the treatment of the particles competition being managed by means of a multistep code. The discrepancies at the high energy side remain for the α-particles.

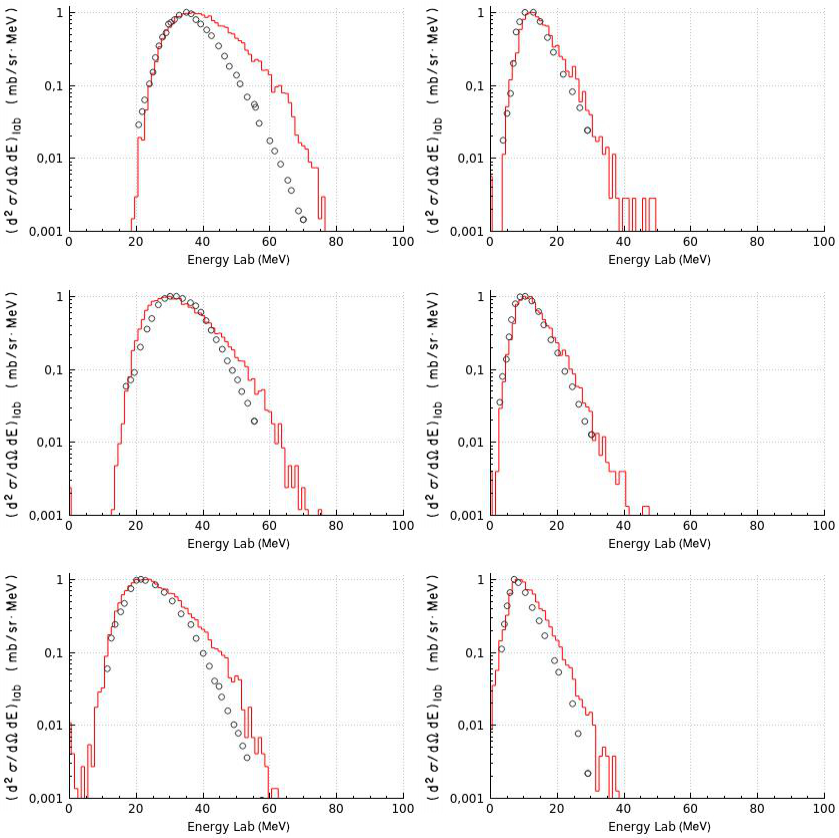

Figure 3.1: Evaporative energy spectra in the 190 MeV ^{40}Ar + ^{27} Al reaction. The α-particle (left) and proton (right) spectra at different laboratory angles : 10 °, 30 ° and 45 ° from top to bottom, respectively. The red lines and dots represent the calculations and the experimental data, respectively. All the spectra have been normalized to the maximum.

In Fig. 3.2 the proton and α-particles angular distributions are compared with the calculations. The calculations have been performed using the same parameters as for the energy spectra but assuming a velocity of centre of mass egual to zero, then the resulting angular distributions have been normalized to the experimental ones at $\theta_{cm} = 90°$. This normalization has been perfomed in order to better evidence the variation of the anisotropies due to rotational energy and moment of inertia

characterizing the compound nucleus at different stages of the evaporative cascades. Irrespective of the charged particle considered, we observe larger anistropies in the calculations. We have to notice that such effects are present in a similar manner also in the proton distributions differently from what it has been observed for the energy spectra. This indicates a smaller moment of inertia with respect to the experimental one, and consequently the presence of a nuclear deformations. This conclusion is in agreement with the observation made for the energy spectra and strongly motivates our analysis in which we introduced the nuclear stratosphere.

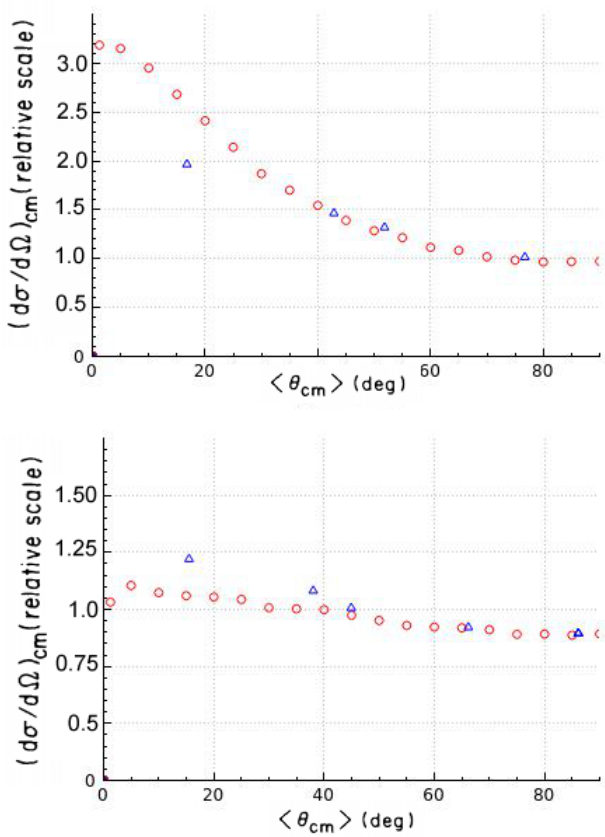

Figure 3.2: Angular distribution of the evaporative charged particles in the 1190 MeV ^{40}Ar + ^{27} reaction: α-particles (top) and protons (bottom). Blue triangles represent the experimental points and the red dots represent the results of calculations. The calculated curves have been normalized to the data at 90° .

3.1.2 Nuclear Stratosphere and deformation

The analysis of experimental observables in the framework of SSM evidenced the discrepancies produced by assuming the emission from spherical nuclei for the reaction under investigation. La Rana and coll. [Lar87] tried to solve this problem by introducing deformation effects. Unfortunately, the use of a single step code and TCs based on local and unextended systematics limited the possibility to provide a real-

istic description of the process and to reproduce simultaneusly full dataset. A more detailed and flexible description of the nuclear shape which allows to make a step forward can be reached by means of the nuclear stratosphere and global TCs. Thus, a grid of calculation has been carried out to find the h and b parameters reproducing the experimental data.

The h and b parameters have been varied in the range $0.01 - 0.15$ and $1 - 4fm$, respectively. The best results has been achieved with the combination $h = 0.077$ and $b = 2.6\ fm$. In this calculation a deformation with a ratio b/a [Bec01, Vie88] (ratio major to minor axes) up to 1.7 at $J_{ER} = 46\ \hbar$ has been included. This value can be considered as normal deformation being in line with rotating liquid drop model predictions for similar nuclei (see Ref. [Pue77]).

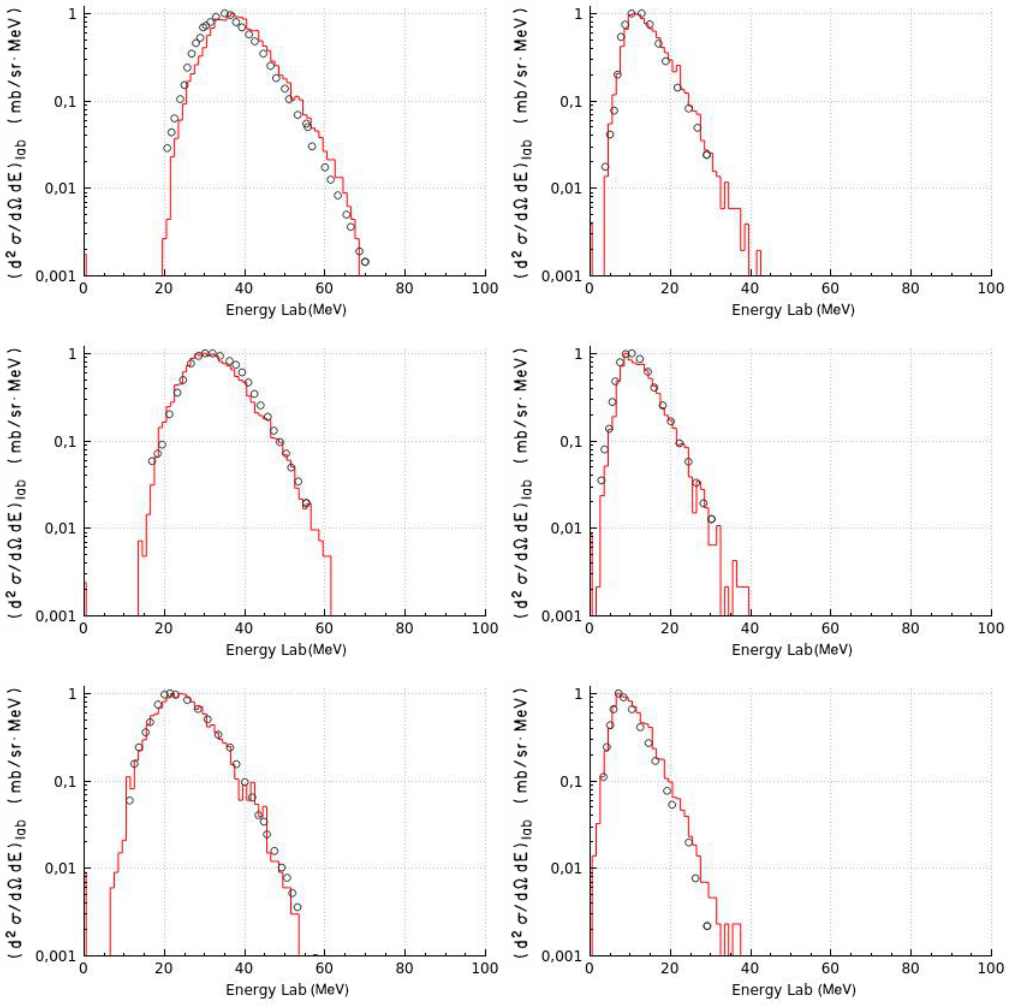

Figure 3.3: Evaporative energy spectra in the 190 MeV ^{40}Ar + ^{27}Al reaction. The α-particle (left) and proton (right) spectra at different laboratory angles : 10 °, 30 ° and 45 ° from top to bottom, respectively. The red lines and dots represent the calculations and the experimental data, respectively. All the spectra have been normalized to the maximum.

The use of the nuclear stratosphere solved the problem concerning the high energy side of α-particle spectra and allows to obtain a good agreement with energy spectra irrespective of the angle and particle type. The comparison with data is shown in

Fig.3.3.

The most relevant results we achieve for this compound system are 1) the simultaneous reproduction of proton and α-particles energy spectra using a single set of model parameters, 2) that the nuclear stratosphere is an essential ingredient and 3) that the experimental data can be reproduced without having to rely on exceptionally large deformations, which can be questionable.

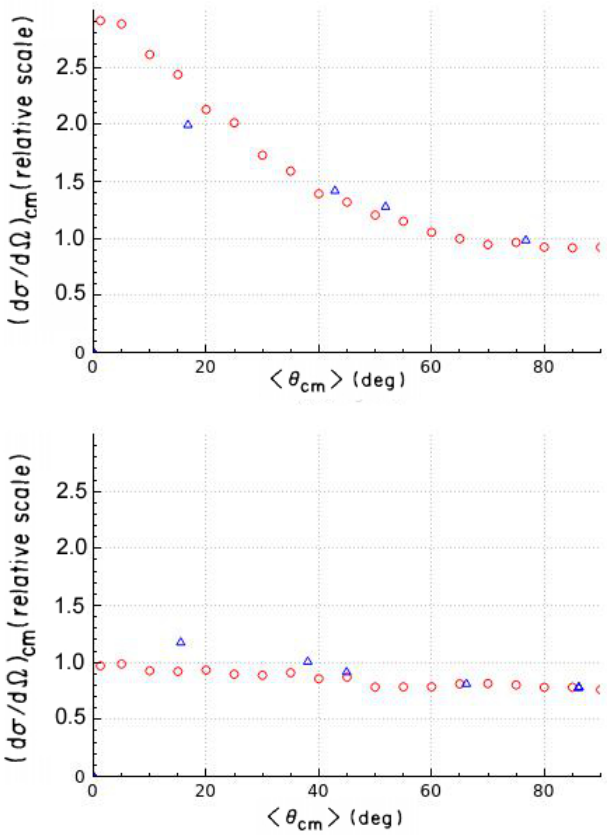

Figure 3.4: Angular distribution of the evaporative charged particles in the 190 MeV ^{40}Ar + ^{27}Al reaction: α-particles (top) and protons (bottom). Blue triangles represent the experimental points and the red dots represent the results of calculations. The calculated curves have been normalized to the data at 90° .

This new model improves also the reproduction of the α-particles angular dis-

tribution and the difference is reduced to a factor 3, whereas the quality of the agreement is unchanged for the protons. A larger deformation had to be excluded because it would produce a general worsening for what it concerns the energy spectra as well as for the angular distribution of proton.

Further improvements can be achieved by using a finer step in the calculation grid. However, the main conclusions about the substantial improvements do not change. The evident step forward is to be ascribed exclusively to the implementation of the nuclear stratosphere model.

In order to disentangle the interplay between the level density parameter " a " (the so called little a) and the deformation contributions, both affecting the shapes of the energy spectra, the differential multiplicity ratios between α-particles and protons at different polar angles ($dM_\alpha(\theta)/dM_p(\theta)$) have been considered. This observable is influenced by the protons and α-particles competition. Therefore, it represents an observable which can provide a further constraint to the model parameters. This quantity is different from the angular distribution since it represents an absolute and not relative datum, which provides a more quantitative indication of how much energy is dissipated through the emission of the different particles. The difference between the calculations and the experimental data ranges from 25% to 40% in the case of the standard statistical model, while it is strongly reduced when the model with nuclear stratosphere is introduced, and becomes 17% less at 10 ° and 14% at 45 °.

	Exp	SSM	Stratosphere
$dM_\alpha(10°)/dM_p(10°)$	1.5	2	1.75
$dM_\alpha(45°)/dM_p(45°)$	0.6	1	0.7

Table 3.1: Differential multiplicity ratios between α-particles and protons at different polar angles for $\theta = 10° - 45°$. Experimental data are compared, calculation with Standard Statistical Model and Statistical Model with Stratosphere.

On these grounds, we conclude that the nuclear stratosphere represents an essential and well-suited model to describe the decay of the $67Ga^*$ at high excitation energy of 97 MeV.

3.2 The reaction ^{30}Si + ^{30}Si

To validate the successful approach described before for ^{67}Ga*, the 120 MeV ^{30}Si + ^{30}Si reaction, with similar mass has been analyzed. For this reaction, producing the compound nucleus ^{60}Ni at the excitation energy of 75 MeV, α-particles energy spectra were measured only. The reproduction of experimental data was not achieved by La Rana et al. within the framework of SSM but only by introducing even larger deformations ($\frac{b}{a} = 3$)Ref.[Lar88]. In light of this we analyzed the same data using the improved version of LILITA code and the two steps approach described before. Also for this system a grid of calculations has been performed varying h and b parameters in the range $0.01 - 0.15$ and $1 - 4fm$,respectively. Calculations considering spherical shapes of emitters provided a well reproduction of the experimental data.

Results obtained using the standard statistical model are shown in Fig. 3.5. We observed that the α-particles energy spectra are shifted at higher energies with respect to the measured data. Accordingly to the previous discussion this behavior suggests the presence of deformation in the emitting nucleus.

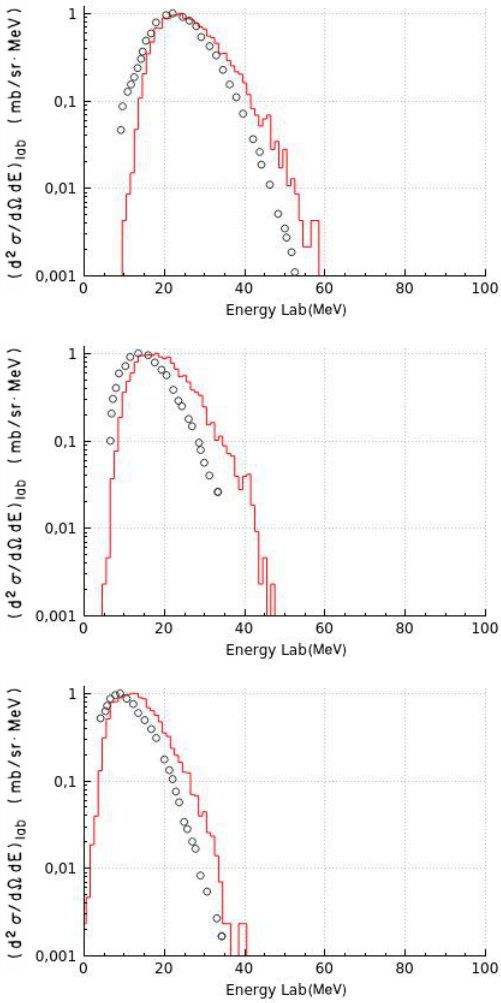

Figure 3.5: Energy spectra of α-particles from the reaction 120 MeV ^{30}Si + ^{30}Si compared with standard statistical model predictions. From top to bottom are the spectra for angles 35 °, 55 ° and 75 °. The continuous red line represents the distribution obtained by the simulation whereas the empty dots are the experimental data.

We then proceeded with a further simulation using the stratosphere model. A grid of calculations has been used to find the best h and b parameters to simultaneously reproduce the experimental data. The best result was obtained for $h = 0.055$ and

$b = 2\ fm$. In Fig.3.6 we can appreciate the good reproducibility of experimental data.

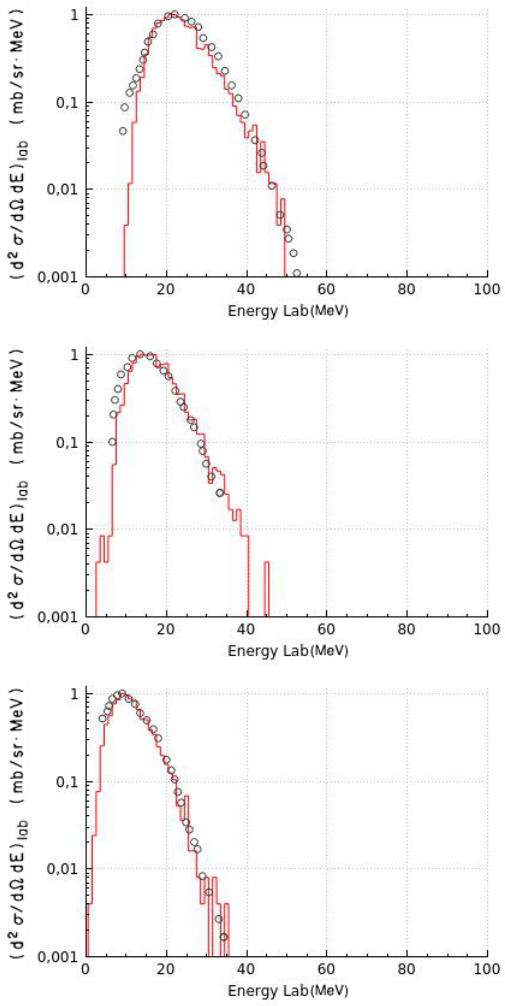

Figure 3.6: Energy spectra of α-particles obtained by stratospheric model. From top to bottom the spectra for angles 35 °, 55 ° and 75 °. The continuous red line represents the distribution obtained by simulation while the empty dots are the experimental data.

It is important to underline that the good agreement with the experimental data has been achieved only with the introduction of the stratosphere model without any

recourse to possible deformations. Therefore, this new version of LILITA seems to be well suited to provide a more realistic description of the evaporation decay occurring in nuclei with high excitation energy and high angular momenta.

3.3 655 MeV ^{60}Ni + ^{100}Mo

In order to further check the importance of the stratosphere model approach, we have searched for a heavier compound system for which a large set of observables were measured. We considered the reaction 655 MeV ^{60}Ni + ^{100}Mo forming the nucleus $^{160}Yb^*$ with excitation energy of about 280 MeV and $J_{ER} = 63\ \hbar$ [Gon90, Cha01]. In our simulation we follow the same approach, namely first we start by using the spherical statistical model (so called standard statistical model) and afterward we check the effect of introducing deformation and stratosphere models.

3.3.1 Analysis based on simulations with Standard Statistical Model

For the calculations of the available measured observables we used LILITA considering a spherical nucleus and imposing $a = \frac{A}{13.8}$. This value of the little a is the one used by Charity et al. We have to stress, however, that this value is not justified by the general systematics shown in the first chapter in Fig.1.4. It was used by the authors with the only task to attempt to reproduce their data.

In Fig. 3.7 the energy spectra obtained with the standard statistical model implemented in LILITA are shown.

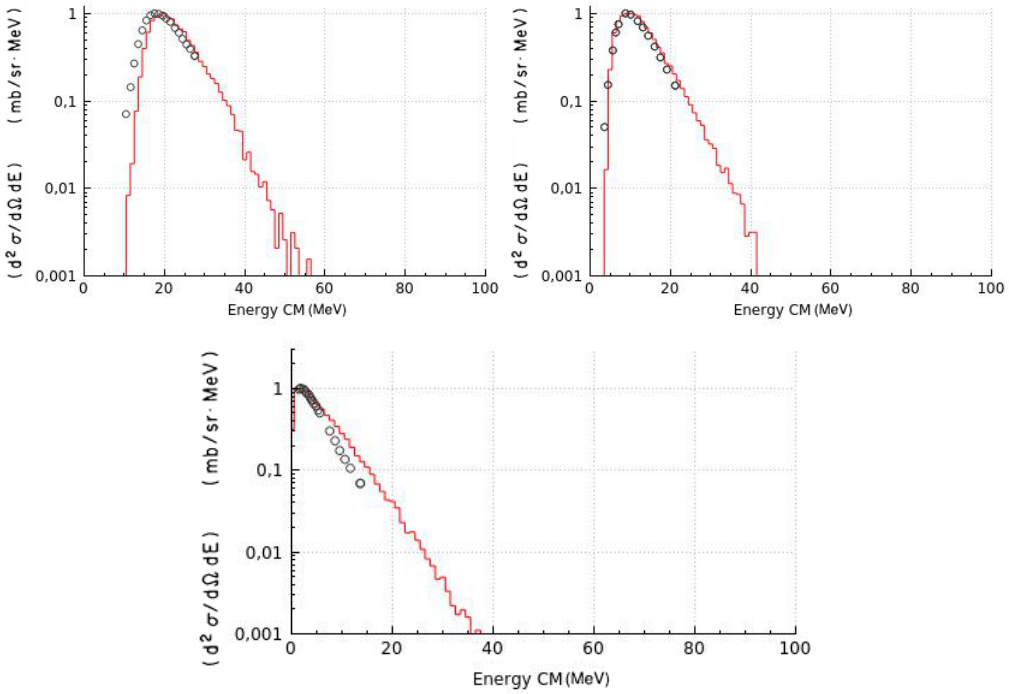

Figure 3.7: Energy spectra of α-particles, protons and neutrons. On the left at the top the spectra of the α-particles, whereas on the right the protons. Neutrons are below. The points indicate the measured data while the red continuous line show the data obtained by the simulation. The value of little "a" chosen, much lower than the systematics value, has the effect of increasing the higher energy emission of neutrons. This effect is milder in the case of α-particles.

Unlike the work in Ref. [Cha01], in our calculation, we have not introduced any deformation. The lower value of little " a" sensibly increases the emission of the high energy neutrons. This effect is milder for the α-particles but the absence of deformation means that the α-particles distribution is not adequately reproduced at low energy while the neutrons diverges from the experimental data in the high energy part of the distribution. This behavior confirms that the use of the level density parameter equal to $\frac{A}{13.8}$ has no actual physical meaning but is a mere expedient to mock the nuclear deformation to reproduce the energy distributions.

This last statement is confirmed by the comparison of the particle multiplicities of the reaction we calculated and that are shown in the Tab. 3.2.

Table 3.2: Light particles measured multiplicities for the ^{60}Ni + ^{100}Mo reaction [Cha01] compared with the LILITA SSM predictions .

	Mn	Mp	Mα
Exp.	10.2±0.7	4.8±0.8	1.9±0.1
Cal.(LILITA)	8.3	4.7	2.9

The increase in the high-energy neutrons actually reduces their multiplicity and, in the balance of particle emission competition, favors the emission of α-particles which are in fact overestimated with respect to the experimental data. The good reproduction of the proton energy distributions translates in this case also into a good reproduction of their multiplicity.

3.3.2 Nuclear Stratosphere

By introducing the nuclear stratosphere model and fixing the only free parameters $h$and b at $h = 0.01$ and $b = 4.0\ fm$, we can reproduce exceptionally well the whole set of data. Energy spetra are show in Fig.3.8. It is important to remark that this result was obtained by using the systematics value $a = \frac{A}{8}$. No form of nuclear deformation was included.

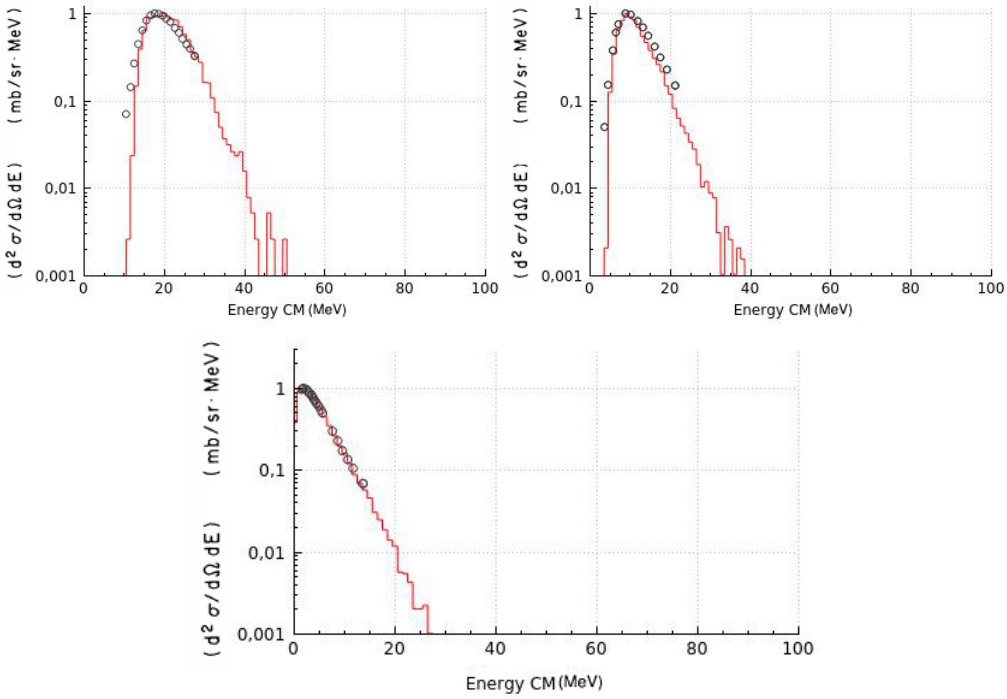

Figure 3.8: Energy spectra of α-particle, protons and neutrons. On the left at the top the spectra of the α-particles;on the right the protons. Neutrons are below. Dots indicate the measured data while the red continuous line shows the data obtained by the simulation with $h = 0.01$ and $b = 4.0\ fm$.

In Tab. 3.2 the multiplicity of the particles emitted are reported. With respect to the calculations observed in Tab.1.1 there is a clear improvement, especially in the prediction of the neutron multiplicity. In the case of the reaction under examination, the use of the stratosphere model seems to compensate for the weak predictability of the standard statistical model as what it concerns with the multiplicity of light particles emitted.

Table 3.3: Light particles multiplicities for the reaction ^{60}Ni + ^{100}Mo[Cha01] compared with statistical model predictions including the stratosphere model.

	Mn	Mp	Mα
Exp.	10.2±0.7	4.8±0.8	1.9±0.1
Cal.	10.8	5.3	1.7

A further confirmation of the goodness of the model calculations is the comparison with the experimental data regarding the multiplicity of the α-particles as a function of the angle of detection of the residue. In Fig.3.9 we show that the differences never exceed 20% while the difference with calculation obtained without stratosphere reach up to 50%.

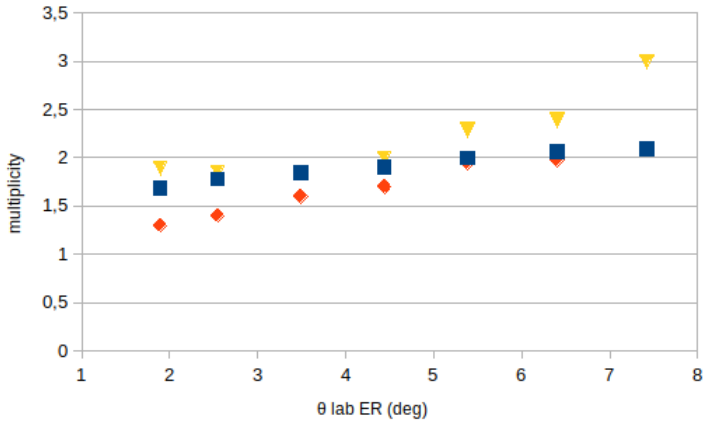

Figure 3.9: Experimental evaporative α-particles multiplicities extracted as a function of the detection angle of evaporation residue (in blue). The orange and yellow points shows multiplicity predicted by using statistical model with stratosphere and without stratosphere, respectively.

3.4 Temperature vs Stratosphere: an empirical law

From the analyses discussed above we can conclude that with the statistical model which includes the stratosphere model it is possible to reproduce, with very good accuracy, many evaporative channel observables in three compound systems where the SSM is known to fail. This default of the SSM has been a pending problem since the 80's. From our analysis it seems that the stratosphere model might constitute therefore an important missing ingredient. However, it is worth to note that none of the two parameters h and b appearing in the Batko and Civitarese model has a predicted dependence on the properties of the evaporating nucleus. In our simulations they were treated as free parameters. The values indicated in the previous paragraphs for h and b were in fact extracted through the use of a calculation grid and by searching for the best agreement with the full set of data for each compound system.

In order to explore the predictive power of the model proposed by Batko and Civitarese, and in the lack of a model for h and b, a possible strategy is to check if there is a general trend, an empirical law that may link the parameters of the stratosphere derived from the comparison with the available data to quantities such as temperature and/ or other physical characteristics of the CN. Fig. 3.10 show the trend lines obtained reporting h as function of the mass and b as function of the initial temperature of the CN. The filled points are the one extracted from the analysis of the three reactions above. The filled lines are a guess of a possible trend in both plots.

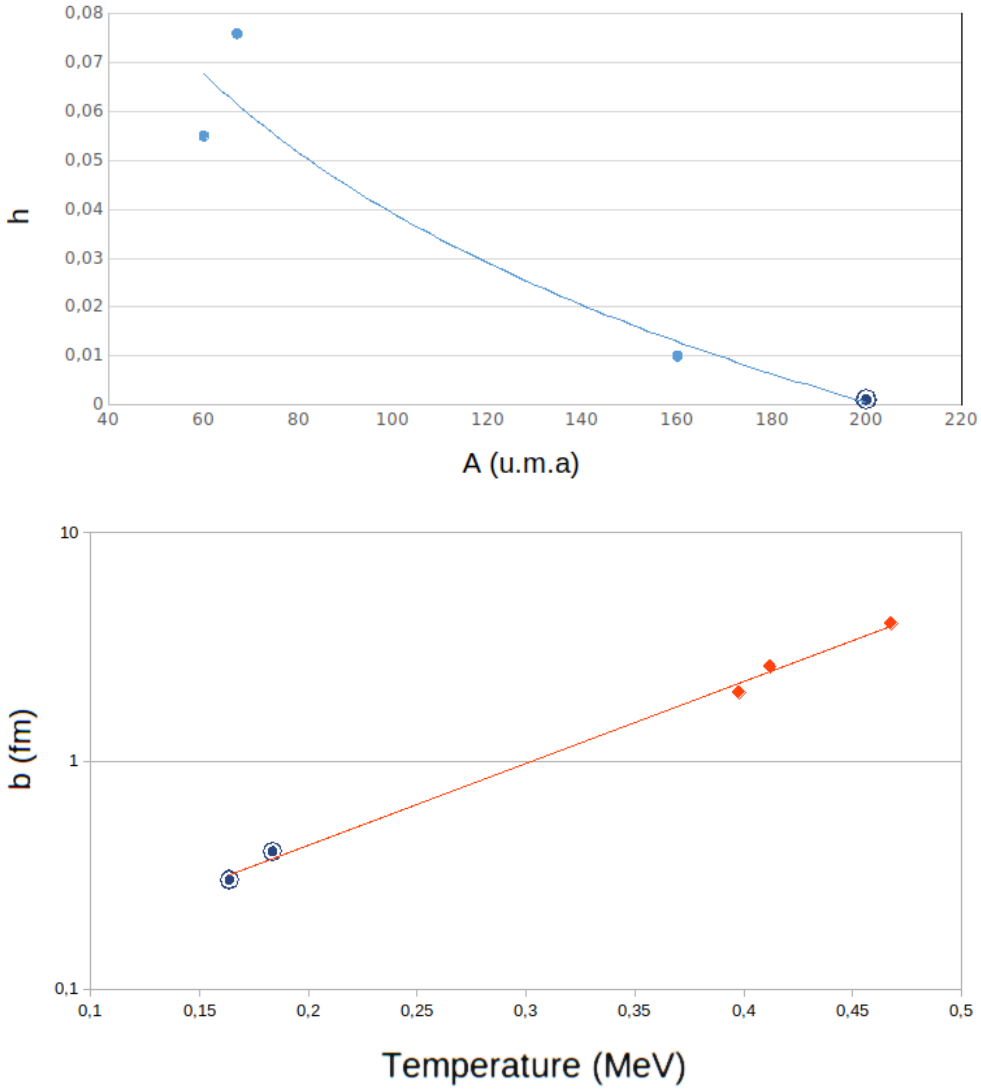

Figure 3.10: Trend of the parameter h as a function of the mass number of the compound nucleus (top) and trend of b as function of initial temperature of the CN (bottom). The filled points are the values extracted from the analysis of the CN performed above. Lines are drawn as a possible empirical trend based only on those three filled points and serve to guide the eyes. The empty points refer to ^{200}Po*.

It is possible to deduce that h seems to decrease as the CN mass increases, whereas

the value of b seems to grow exponentially as the initial CN temperature increases. Clearly, tests on more systems should be continued to increase the number of points on these plot.

To confirm these trends we decided to analyze the reaction: $340-360\ MeV$ ^{84}Kr + ^{116}Cd $\rightarrow$^{200}Po*[Han87], which refers to a heavier system, at lower temperature, and for which neutron multiplicities were measured only. From the trends drawn in Fig.3.10 the values of h and b for ^{200}Po at E* = 43 and 55 MeV are $h = 0.001$ and $b = 0.3$, and $b = 0.4$ fm for the two excitation energies.

With these fixed values we performed the calculation of the evaporative cross sections for the channels 2n, 3n and 4n shown in Tab.3.4. Cross sections are normalized to the most populated channel (3n channel at 43 MeV and 4n at 55 MeV) because the fusion cross section was not measured and not available elsewhere.

E* = 43 MeV			E* = 55 MeV		
Channel	Exp.	Calc.	Channel	Exp.	Calc.
2n	0.26±0.08	0.18	2n	0.14 ±0.04	0.17
3n	1	1	3n	0.61±0.11	0.78
4n	0.17±0.05	0.16	4n	1	1
1n1p	?	0.01	5n	0.08±0.01	0.09
2n1p	?	0.04	2n1α	?	0.02
1n1α	?	0.004	2n1p	?	0.06

Table 3.4: Cross sections of emission channels 2n, 3n and 4n measured in the reaction ^{84}Kr + ^{116}Cd $\rightarrow$^{200}Po* and computed by using the stratosphere model. Cross sections are normalized to the most populated channel (3n channel at 43 MeV and 4n at 55 MeV) because fusion cross section was not measured and not available elsewhere. (left) data for excitation energy equal to 43 MeV; (right) data for excitation energy equal to 55 MeV.

It is possible to observe that the calculated cross sections obtained are extremely close to the experimental data, for both excitation energies. This result supports the fact that the empirical trend found on the basis of only three reactions represents

already a good guess for the dependence of the stratosphere model parameters from the CN temperature and mass. In addition, we note that the compound nucleus ^{200}Po* represents a case far from the three reactions analyzed above and on which the empirical trend is based, both in mass and temperature. Clearly, this analysis would require additional simulation work with the code developed in this thesis but it reasonably shows that the extraction of an empirical law is possible. This conclusion would in principle trigger additional theoretical work on the subject and experimental work as well to measure other unknown decay channels in the reactions $340 - 360\ MeV\ ^{84}\mathrm{Kr} + {}^{116}\mathrm{Cd} \rightarrow {}^{200}\mathrm{Po}^{*}$.

Summary and conclusions

In this work the effects of a possible description of a nuclear stratosphere on the evaporation process has been studied. We first provided an overview of the standard statistical model and its main ingredients. Three different evaporation fusion reactions, characterized by high temperature and angular momentum values, were examined. The inability of the standard statistical model to reproduce some physical observables was highlighted. The observed differences suggest the presence of a distention of the nucleus not reproducible in any way by the standard model unless forcing, only in some cases, the model itself in an unrealistic way. Using the model suggested by Batko and Civitarese, we have therefore introduced the elements of the nuclear stratosphere into the statistical model.

A quick analysis of the variations induced by the use of different parameters of the nuclear stratosphere on two system types (light and heavy masses) allowed us to learn about the effects of the introduction of this model on the various calculated observables. This exercise was very useful in order to acquire a knowledge that could teach us about the use of this tool to overcome the defaults found in the standard statistical model.

In the case of the reaction 190 MeV ^{40}Ar + ^{27}Al, the Standard Statistical model was not able to reproduce the spectrum of protons and $\alpha-$particles unless by forcing

a straight reduction of the specific emission barriers for each charged particle considered. Also the simulated angular distributions showed evident differences with the experimental data. The use of the stratosphere model improves both the reproduction of energy distributions and the angular distribution of charged particles without having to resort to an unrealistic deformation of the nucleus or artificial reduction of the barriers.

For the reaction 120 MeV ^{30}Si + ^{30}Si only energy spectra of the $\alpha-$particles were measured. Also in this case, in the original paper by La Rana et al., for a close reproduction of the energy spectra it was necessary to resort to the use of an unreasonable large deformation of the nucleus. The use of our LILITA evaporative multistep code, with updated transmission coefficients, reduced the gap between the experimental data and the calculation, but did not compensate it completely. The addition of the stratosphere led to full overlap of energy distributions at various laboratory angles with the collected experimental data.

For the third reaction analyzed in Gonin et al., it was also reported that both multiplicities and energy distributions could not be reproduced by the SSM. In this case, which provides the largest number of measured observables than the other two reactions, the use of the stratosphere model has produced calculated data much more closer to the experimental ones without using, even in this case, any specific customization of the parameters except for h and b stratosphere model parameters.

From the three reactions analyzed, it was in addition possible to derive an empirical law for the parameters h and b which appears to be well suited to predict the behavior of the stratosphere in other reactions. This case was demonstrated by the reaction producing ^{200}Po*.

The use of the stratosphere model in the statistical model seems to be quite

promising as it solves a long standing problem. Further work is however necessary to verify the potential of the model to reproduce data from a larger set of reactions. This process would further clarify if an empirical laws may exist for the parameters b and h, and would hopefully trigger further experimental and theoretical work.

Appendix

In this Appendix the new features of LILITA_N18 are described. The new version of the evaporative multistep code LILITA [Gom81] used in this study does not include only the nuclear stratosphere model and global transmission coefficients for neutrons, protons and alpha particles, described in details in the Chapter 2, but also many technical developments.

A large effort was devoted to the construction of the graphical interface that simplifies the procedure to run calculations and offers new options such as the possibility to monitoring the results or to perform grid of calculations by selecting the intervals of parameters to be chosen to scan. Another important aspect consists in the parallelization of the code. This aspect is crucial because it can reduce the computation time that sometimes can last weeks. The new version of the code can share the calculations among the different cores available on the existing machines. This peculiarity paves the way for the future development of the code that can simultaneously run on machines connected in a standard network. This option has been successfully tested and will be implanted in the final release of the code. This solution can be very useful to calculate the observables produced in the rare decay channels, as those usually of interest for the nuclear structure studies (e.g. [Hüy16]). Future developments will be devoted to the implementation of the detection geome-

try. With this aim a series of routines have been developed during this Ph.D. work in order to realize a complete tool-box able to reproduce large set of observables by taking into account the experimental conditions.

LILITA

LILITA [Gom81] is a computer code based on the Monte Carlo approach simulating the particle emission in the evaporative cascades of the CN decay. The code calculates the energy spectra and angular distributions of the particles providing an event-by-event output. The particle emission probability, accordingly the Statistical Model (see description in Chapter 1) is calculated using the transmission coefficients and the level density of the evaporation residue.

To run the code it is required to provide the number of stories to generate and input parameters describing the reactants, the compound nucleus formed and the reaction conditions:

- the mass and atomic numbers of projectile, target and compound nuclei (A_0, Z_0);
- the maximum angular momentum (J_0) of the CN;
- the projectile energy in the laboratory system Elab and the compound nucleus excitation energy (E^*);
- the fusion cross section. Several options that can modify the features of the CN were already existing in the previous updated version LILITA_N11:
- different parameters of the level density ("A/a");
- different radius parameter for the calculation of the moment of inertia with the nuclear approximation of the nucleus to a rigid sphere;
- deformation parameters;

• prescriptions for the transmission coefficients based on the Optical Model, Fusion Systematics [Vaz84] and Ingoing Wave IWBCM [Kil92].

Once these initial parameters are set, the code proceeds to calculate for each step of the evaporative cascade the mass A, the charge Z, the excitation energy E^* and the angular momentum J of the residual nucleus. If the residual nucleus has sufficient amount of excitation energy to emit another particle, the code simulates once again the emission of a particle. At each k-th step of the cascade the code calculates the A_k, Z_k, $E^*{}_k$ and J_k of the residual nucleus. The first two quantities depend on the type of emitted particle, whereas the excitation energy and the total angular momentum depend on the angular momentum l_k and the kinetic energy ϵ_k carried out by the emitted particle.

$$E_{k-1} = E_k + E_{sep} + \varepsilon_k$$

$$\vec{J}_{k-1} = \vec{J}_k + \vec{l_k}$$

Each step is controlled by the emission probability $P_k(E_{k-1}, J_{k-1}, (\varepsilon_k, l_k), E_k, J_k)$, of a particle i_k, with moment l_k and energy ε_k from a nucleus with total angular momentum $\vec{J}_{k-1}$ and excitation energy E_{k-1}.

A_0, Z_0, E_0^* and J_0 are the starting points for the simulation of the evaporative cascade. They represent the mass, charge, excitation energy and momentum of the CN. The A_0, Z_0 and E_0^* are fixed input parameter of LILITA, while direction and modulus of J_0 are randomly generated using the inverse transformation method. The direction of $\vec{J_0}$ is perpendicular to the direction of the beam and its azimuth angle is given by:

$$\phi = 2\pi\eta$$

where η is a pseudo-random number in the range [0,1]. The modulus of the $\vec{J}_0$ is generated according to a triangular distribution using the following relation:

$$J_0 = \frac{1}{2}\sqrt{1+\eta[(2J_{max}+1)^2-1]} - 1 \tag{3.1}$$

The next step of the code is the evaluation of the emission probability of a particle i, of angular momentum l_i and energy ε_i, from the CN of energy E_0 and angular momentum J_0. The emission probability distribution is given by the expression:

$$P_i(E_0, J_0) = \sum_{l_i}^{l_{max}} \sum_{J_1=J_0-l_i}^{J_1=J_0+l_i} \int_{\varepsilon_{min}}^{\varepsilon_{max}} \frac{P_i(E_0, J_0, (\varepsilon_i, l_i), E_1, J_1)}{P_{tot}} d\varepsilon_i \tag{3.2}$$

l_{max} , ε_{min} and ε_{max} are valuated in a defined range of values that depends on the particle type.

The level density is evaluated using the Fermi gas expression given, by 1.4, whereas the transmission coefficients are evaluated using the optical model and a set of parametrizations of the latter. Using 3.2 the code generates the emitted particle i, its angular momentum l_i, the kinetic energy in the center of mass ε_i, and A_1, Z_1, $\vec{J}_1$ and E_1^* are determined. Afterwards the remaining excitation energy of the residue is compared to the emission threshold energies for the different type of particles. If the energy is sufficient for the emission of a further particle code repeats the same procedure as before with different initial conditions for the next evaporative step, otherwise the cascade calculation terminates and the event is stored on the disk. All the information about the kinematics of particles (the three velocity components, kinetic energy and angular momentum) and evaporation residues (the velocity components and the excitation energy and angular momenta of the CN at each step) are written in the event file.

Evolution of LILITA

LILITA_N18 gives access to all the options included in LILITA_N11 in the period 2006-2012. These options consist in the increase of maximum number of stories per simulation, the possibility of mimic the decay of alpha-cluster nuclei produced in correspondence of narrow resonances [Din16], level density dependence on the isospin with the prescription from Ref. [Al-Q03], and minor ones. In LILITA_N11 the input and output files that have to be managed by the users are formatted text files, where all the reaction conditions and the description of the output files have to be provided. This approach offers the possibility to store the results and save the input files. However, due to the absence of comments/description of the large amount of input variables that have to be changed for each reaction the use of the code is not user-friendly. Therefore, there is the risk to produce errors in the filling of the input cards, which are usually identified later during the analysis of the output file or in worst cases after the filtering of the event file. In LILITA_N18 the main changes can be summarized as:

1. Implementation of graphic interface developed for a simplified inclusion of input variables (for nuclear reaction and compound-nucleus decay descriptions);

2. A graphic on-line monitoring of the simulation results that include the continuous filling of the histograms of the light-particle energy distributions, ER production yields and light particle multiplicities;

3. Parallelization of the code;

4. Possibility to perform grid of calculations by varying the Stratosphere model parameters.

Configuration interface

The first and second cards included in the graphic interface are devoted to the inclusion of the reaction variables, the parameter combinations to lead the evaporative decay process of the compound nucleus, and the parameters to define the information included in the output file. For each variable an explanation is given near the box to fill. The interface gives also the possibility to save the full set of input variables or to load an existing one, in line with the previous version of the code, to make easier the procedure in which only a single variables have to be changed or in case is of interest to change only the reaction keeping the same combination of prescription to describe the decay process.

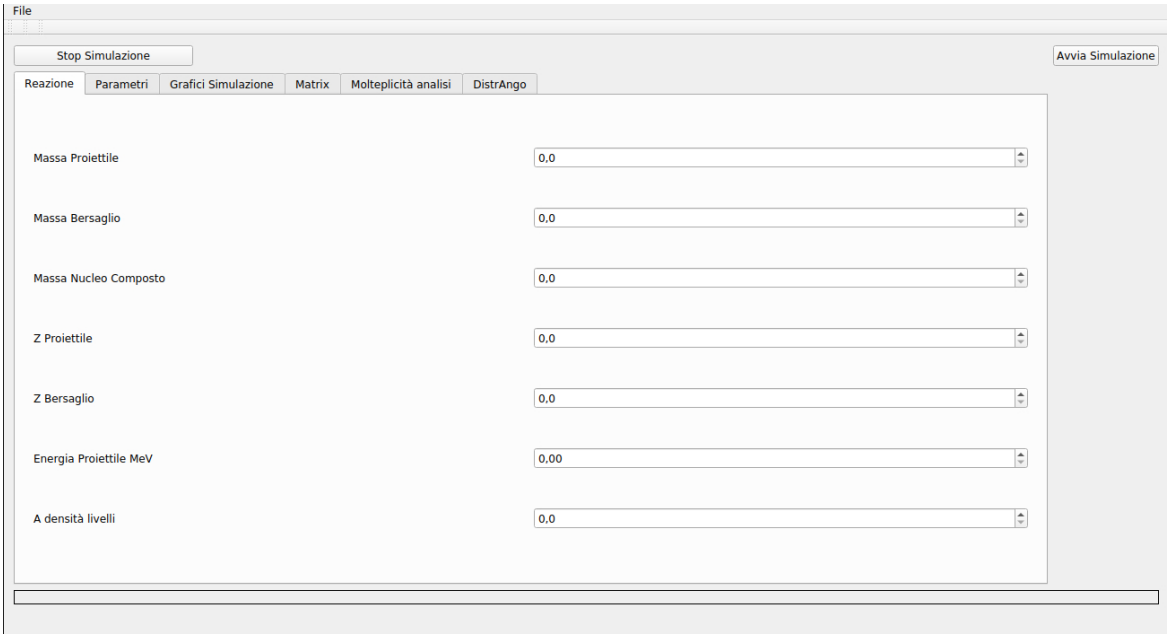

Figure 3.11: Input tab for the reaction parameters in LILITA_N18. On the left are listed the variables that have to be included, on the right the boxes to fill.

In the first tab, shown in Fig. 3.11, are shown the reaction variables to be filled

(e.g. the projectile and target a mass and atomic numbers, the beam energy, the level density parameter, etc.).

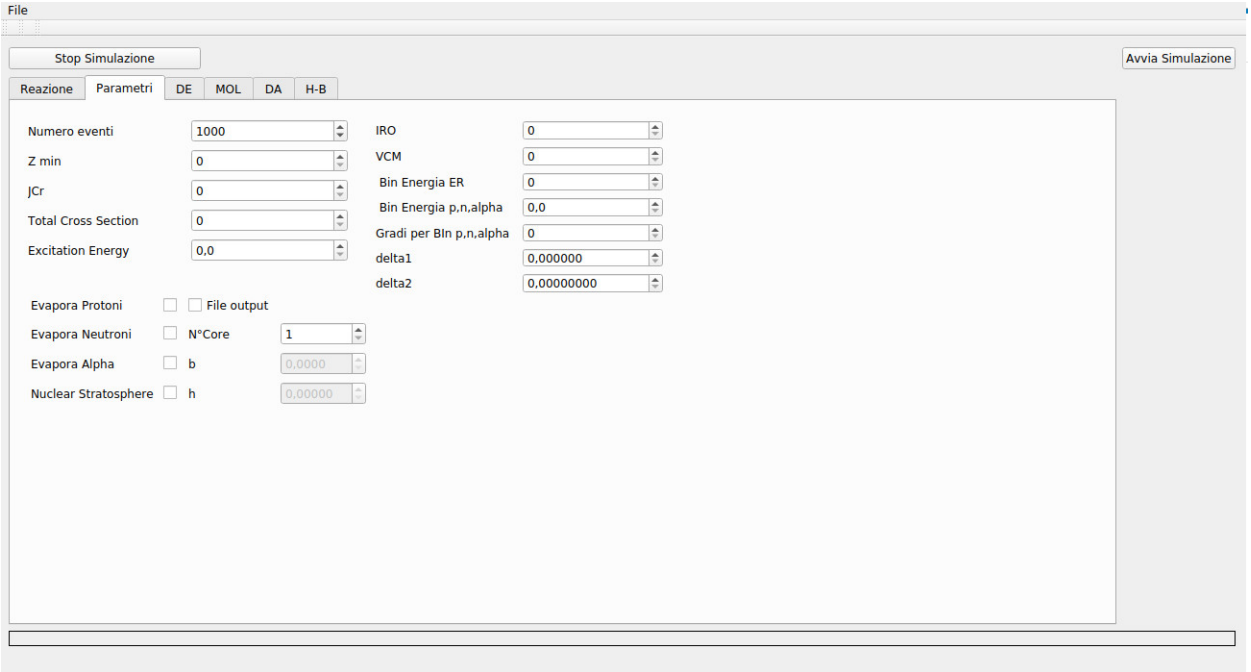

Figure 3.12: Input tab for parameter that characterize the output of LILITA_N18. The input variables are distributed in two columns. On the left of each column are listed the variables that have to be included, on the right the boxes to fill. This card is dedicated to the definition of the number of cascades to simulate; the excitation energy and the maximum fusion cross-section and maximum angular momentum of the CN, and other parameters to define the information included in the output files.

The tab Parametri, Fig.3.12, is dedicated to the description of the CN formed (maximum angular momentum J_{cr}, excitation energy, nuclear deformation, and so on) and to the specific details on the simulations as the total number of stories, the center of mass velocity, the quantities to store in the event and in the output files and plots. If the nuclear stratosphere check box is clicked then it is possible to enter the values of the two parameters h and b. The graphical appearance is the same as

of the previous tab.

On-line monitoring

The LILITA_N18 tab 3 and 4 (DE e MOL, respectively) of the graphical interface are dedicated to visualize a selected series of the observables. The histogram, the values and the 2-D matrix of plot are continuously updated during the simulation. The polar angular range used to build the α-particles, proton and neutron energy spectra as well as the energy binning of these spectra can be modified during the simulations. This option was implemented being very convenient for the comparisons performed in the present work where the experimental data have been collected with detector of different angular coverage in single mode. In Fig. 3.13 the histograms produced by the 190 MeV ^{40}Ar $+^{27}$Al simulated reaction produced in the tab 3 are shown.

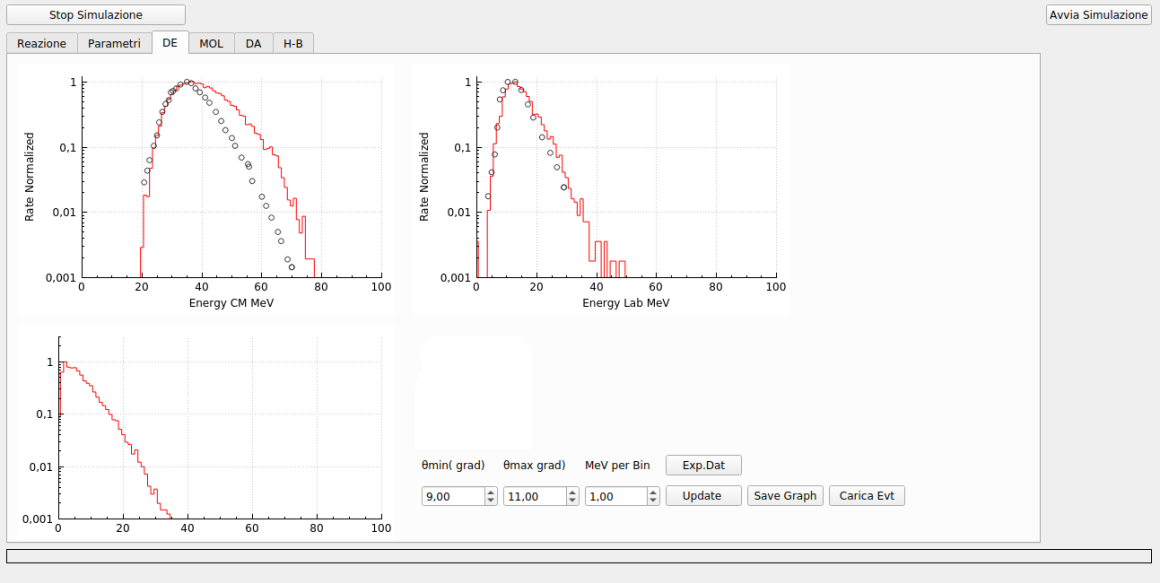

Figure 3.13: Tab DE for the on-line monitoring of the light particle energy distributions histograms of the evaporated: α-particles (top-left), protons (top-right) and neutrons (bottom-left).

The same interface simultaneously monitors on the tab 4 the light particles multiplicities and the Z,N distributions of evaporation residues on 2-D matrix plot and the number of evaporation channels populated in the simulation. On the left side a filter to extract the relative cross-section based on the maximum number of light particles of the channel has been implemented. This is very useful in the case where very rare decay channel observables that require very time consuming simulations that can last weeks or months and in which there is an interest to estimate at some point the expected number of events produced at the end in the simulation. In Fig. 3.14 Tab 4 of the graphical interface is shown as example.

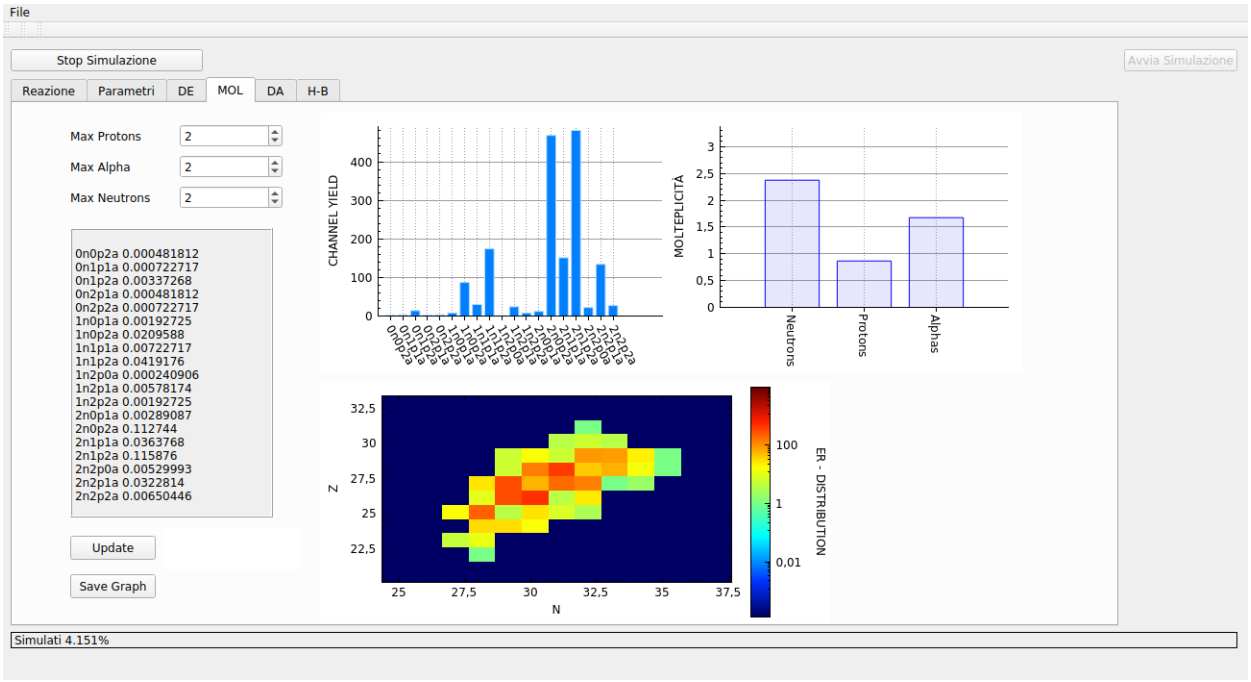

Figure 3.14: Tab with graphical rappresentation the multiplicities, decay channels and distribution matrix of the evaporation residues.

Fig. 3.15 shows Tab 5 that displays the angular distributions of protons, α-particles, neutrons and evaporation residues. The interface allows to select the display ranges for the X and Y axes, and also allows the use a scale factor so that it is possible to overlap the experimental data to determine the increase or decrease in anisotropy.

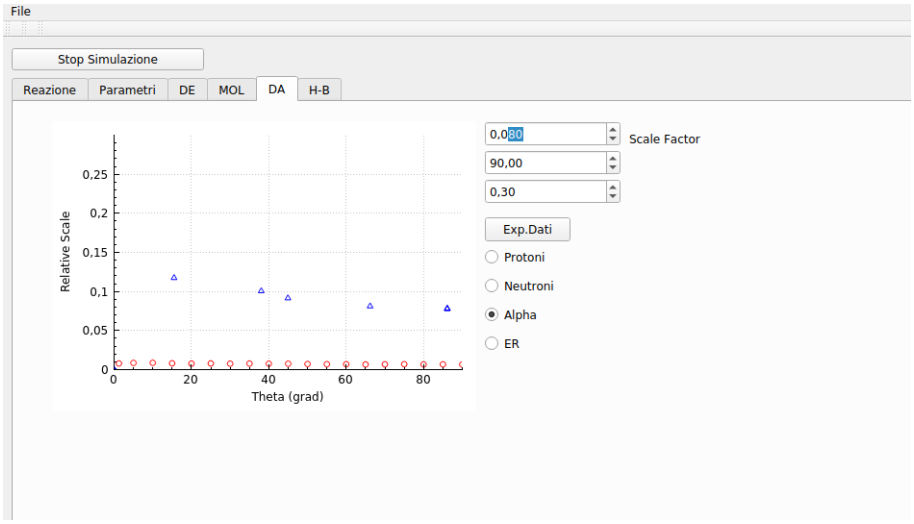

Figure 3.15: Tab with graphic rappresentation of angular distribution. User can select the particle to be displayed and compare the calculated results with external experimental data

The present graphical interface allows also to save the histograms displayed. They can easily be exported in JPG format by pushing the button "Save Graph" included in both tab 3 and 4. If the software is used to determine the better combination of input parameters reproducing the experimental data, these tabs allow to import the experimental data superimposed to the simulations results. This procedure was extensively adopted in this works to produce the plots including the comparisons of the experimental data and simulations reported in Chapter 3.

The Stratosphere Model tab

LILITA_N18 includes the Stratosphere Model in order to test it at low and high nuclear temperature.

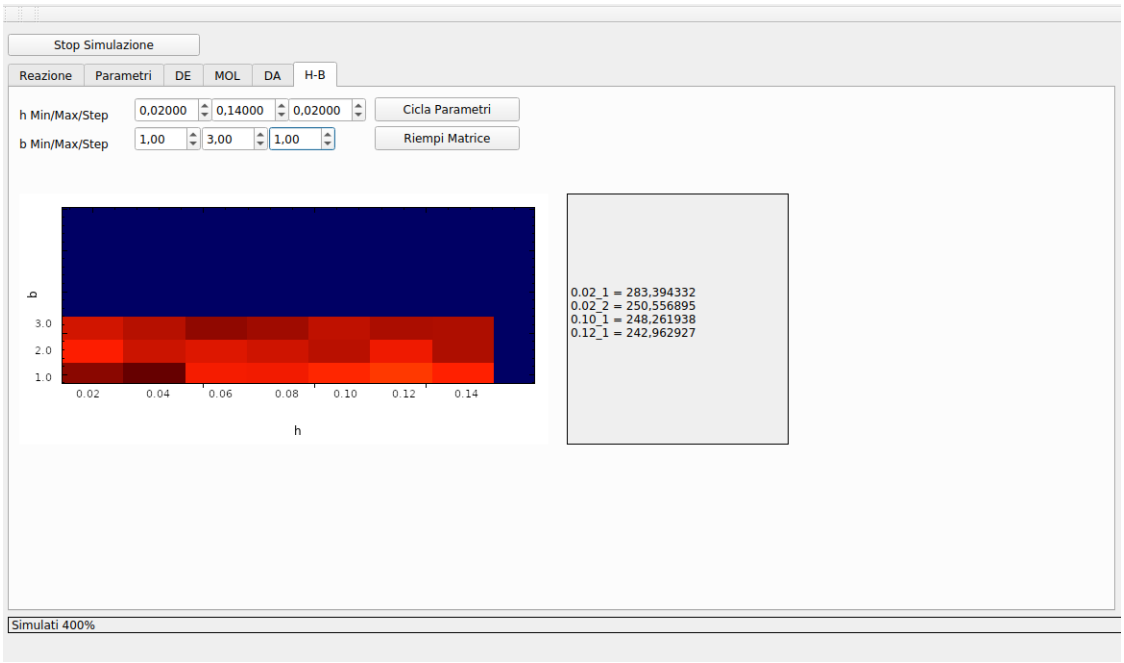

Figure 3.16: Tab H-B included in the graphical interface. In this tab is possible to provide the Stratosphere model combination of parameters describing the density and the extension of the nuclear surface for a single simulation or the intervals of the parameter combinations to run a grid of simulations. On the left the matrix of the results show with various gradations of results obtained, on the right the numerical result.

The tab H-B, shown in Fig. 3.16, is dedicated to the inclusion of the nuclear Stratosphere model parameters h and b, related to the density of the nuclear surface and its extension, respectively. The new interface not only allow to include a single combination of parameters, but also to provide intervals to be scanned with a grid of calculations according the steps defined by the user independently for both b and h. For each b and h combination the code recalculates the TCs on the basis of the nuclear stratosphere description of the nuclear shapes and density. When the grid of calculations is completed, it is possible to use the routines implemented to determine the combination of stratosphere parameters that describe at the best

the experimental data. The experimental data can be superimposed to the on-line monitor plots (series of histograms shown in tab DE). The values, reported in arbitrary units, are the sum of all the differences among experimental and simulated observables. With these values a matrix is filled having h and b parameters on the two axes the values that are used to determine the combinations providing the better reproduction.

Code parallelization and scalability

The LILITA code calculates decay cascades one after the other, therefore it requires large computational time to generate a large number of stories, especially for the reaction in which compound nuclei at high excitation energies are produced. The original code was optimized for the performances of single CPU machine available in the last decades. An important innovation of LILITA_N18 has been the parallelization of the computational procedure for the generation of events. The code automatically identifies the number of cores available on the machine used. The user can therefore choose the maximum number of cores used. The number of stories is then distributed equally between the selected cores. Each run will be initialized with a different seed to generate random numbers, thus ensuring the generation of independent events. To achieve this, the GNU Parallel library[Tan11] was used. The software architecture is thus modified as shown in Fig.3.17

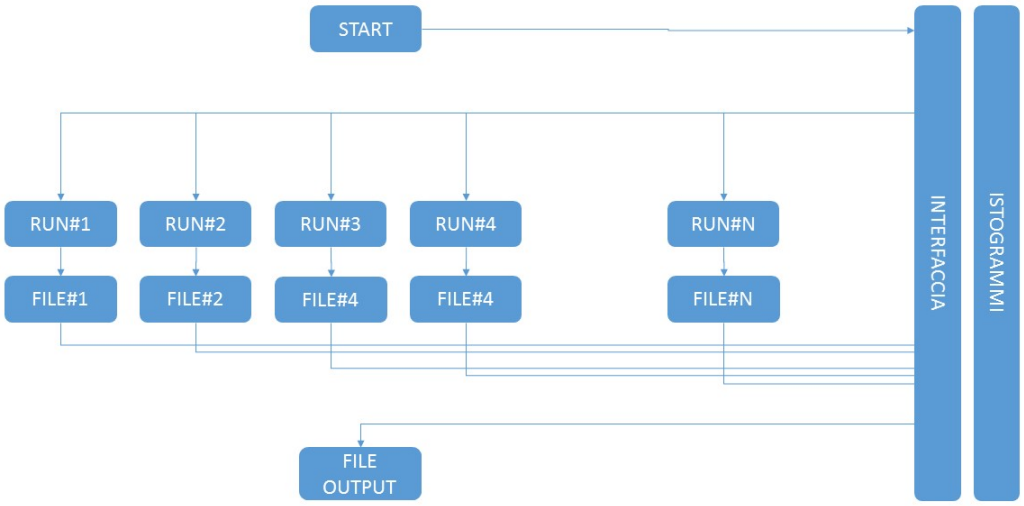

Figure 3.17: Software architecture implemented in LILITA_N18. The interface manages the parallel execution of the code. The calculations are shared on a number of cores whose number is managed by the user. The events produced in the parallel running are collected by the main process of interface that distribute the information: all details are stored in the event file and simultaneously the histograms for the on-line monitoring are updated. At the end of the calculations, the results are summarized in the formatted output file.

The code uses a limited amount of the RAM, in the standard desktop machine, the consumption is usually below 10%, whereas it uses all the available CPU computation power of the single core. The slower procedure of this present version of the code is in the storing procedure, when the results of simulations are written on the event file. The writing procedure on the present code taking place every certain number of events that depends on the size of the bus. During the execution of the code we observe that this process slightly increases the running time especially when the number of core is increased, but there was no need to generate queues. A significant

improvement will be obtained in the next years, when the solid state drives (SSDs) will replace the present conventional hard disk drives (HDDs). The SSDs faster than HDDs in writing procedure up to 2 order of magnitude will provide the optimal conditions to reduce the computational time and overcome the present bottleneck without any further effort. In Fig.4.6 is shown a plot providing an idea about the improvement accessed with the introduction of the parallelization: software execution time vs the number of used cores for a fixed number of events. The trend evidences an inverse proportionality between the execution time and the number of core. Using two and four cores the times are reduced by about a factor 2 or 4, respectively. However, passing from 4 to 8 cores the execution time passes from 5 minutes to 3. In this step the reduction of the execution time is slightly lower than a factor 2, thus the effects produced by the writing speed limit of the internal HDD start to be significant.

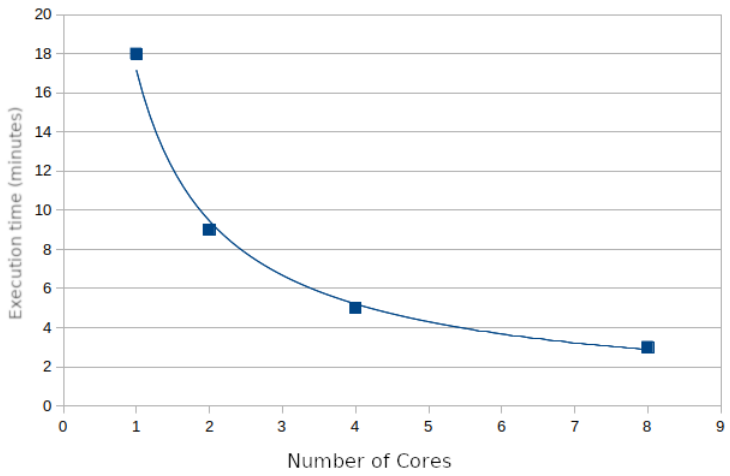

Figure 3.18: Execution time vs Number of cores used. In the 4 cases considered before the same calculation (same reaction and same number of events) has been carried out.

The parallelization is a very useful resource to perform grid of calculations spanning wide intervals for the input parameters or to extract the observables relative to very rare decay channels. The introduction of parallelization has been an essential development to exploit the performances of the actual commercial multi-core machines. The parallelization option gives the opportunity to reduce the execution time by a factor 10 and this number can even increase in the next years. The larger flexibility and the shorter execution time made the new code very useful not only in the phase of analysis, but mainly in the preparation phases of future experiments.

Future implementations

For the next future several developments of the code in stand-alone mode and in combination with a dynamical model including the fusion-fission decay are planned. For each of them as proof of principle several tests or real case have been already made. The first development, successfully used, that we will be soon implemented in the graphical interface consists in the share of the parallel processes on CPU'connected in a local network, as in the case of the parallel running on the different core of a single CPU's. No problems were observed by operating LILITA_N18 on processors with different performances. The inclusion of this option paves the way to the use of the code not only on a local network, but also to exploit the computing resources of the computing centers, as those presently located in many research centers.

The second development in stand-alone mode consists in the inclusions of the detection setup response. A subroutine for this kind of work has been already realized during this Ph.D. work. This subroutine can calculate the energy loss of charged and neutral particles. In Fig. 3.19 a detector made of several elements has been built by means of this routine. The energy release produced by a 2 MeV neutron beam

passing through the setup at the different positions has been calculated and is shown in Fig.3.19(left). The routine provides also detailed information on the scattered beam trajectories exiting from the detection setup.

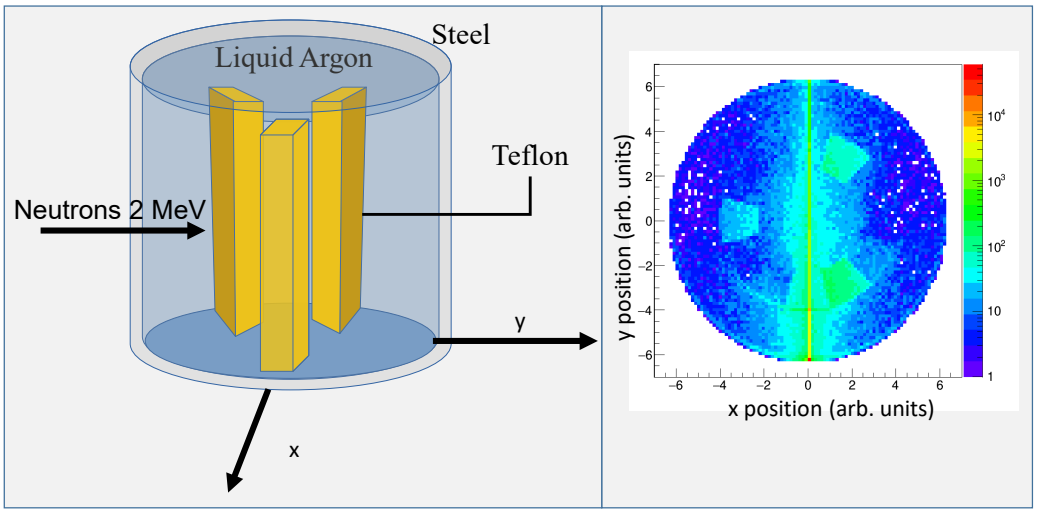

Figure 3.19: Experimental conditions of measurement: a neutron beam of 2 MeV imping on a detector made of several elements made of different materials. Energy response function obtained with the routine *Move* where the different interaction of neutrons on the Teflon and Argon material is evidenced by the different colors which indicate the amount of energy released crossing the detection system.

In the future LILITA_N18 will be coupled with a dynamical model to simulate also the fusion-fission events. The coupling of the previous version of the code has provided very promising results in the reproduction of the experimental data for the intermediate mass systems [Var15] and further improvements in the reproduction of the experimental data are expected.

Bibliography

[Par91] W.E.Parker, M.Kaplan, D.J.Moses, G.La Rana et al.: Phys. Rev C 44, 2 (1991)

[Hod84] P.E Hodgson Rep.Prog.Phys (11984) vol 47 pp 613-654

[Kon03] A.J Koning, J.P.Delaroche Nucl.Phys (2003) A 713

[Per62] F.G.Perey and B.Buck Nucl.Phys. 32 353 (1962)

[Gom81] J.Gomez Del Campo and R.G.Stokstad ORNL-TM 7295, (1981)

[Dos77] T.Dossing : Licentiat Thesus, University of Copenhagen, (1977)

[Eri60] T.Ericson, V.Strutinski.:Nucl. Phys. 8,243 (1958)

[Wei40] V.F.Weisskipf, D.H.Ewing.:Phys. Rev. 57, 472 (1940)

[Lef68] M.Lefort.: Nuclear Chemistry, D. Van Nostrand L.T.D., London (1968)

[Lar87] G. La Rana et al.:Phys. Rev. C 35, 373 (1987)

[Lar88] G. La Rana et al.:Phys. Rev. C 37,1920 (1988)

[Eri58] T.Ericson, V.Struntiski.:Nucl. Phys. 8, 243 (1958)

[Aji86.b] N.N Ajitanad, G. La Rana, et al.: Phys. Rev C 34,3 (1986)

[Aij86] N.N. Aitanand et al.: NIM A 243 111 (1986)

[Sat65] Satchler.:Nuc.Phys 70 177 (1965)

[Hog93] P.E Hogdson,V.Avrigeneau.:Phsy.Rev C, 49 2136 (1993)

[Hog78] Hogdson Nuclear reaction and nuclear structure, Oxford: Clarandon Press (1978)

[Al-Q01] Al-Quiraishi S I et al.:Phsy.Rev C, 63 065803

[Al-Q03] S.I. Al-Quraishi et al., Phys. Rev. C67, 015803 (2003)

[Gon90] M.Gonin,G.Nardelli et al.:Phys. Rev. C, 42,5 (1990)

[Boz89] Bozzolo, G., Civitarese, O., & Vary, J. P. (1989). Physics Letters B, 219(2-3), 161–164

[Bat88] G.Batko, O.Civitarese. Physical Review C, 37 2647(1988)

[Lar88] La Rana, R.Moro et al.: Phys. Rev. C, 37 5 (1988)

[Fro84] P.Frobrich, Phys.Rep.116, 337 (1984)

[Mos85] D.J. Moses et al.:,Z.Phys. A 320, 229 (1985)

[Cho84] R.K.Choudhury et al., Phys.Lett. 143B, 74 (1984); G.Nebbia et al.,ibid.176B,20(1986)

[Bla80] M.Blann, Phys. Rev. C 21, 1770 (1980); M.Blann and T.T.Komoto, ibid.24, 426 (1981)

[Par91] W. E. Parker et al.: Phys. Rev. C, 44 (1991)

[Xin15] X.-W. Su, Y.-L. Han, Internat. J. Modern Phys. 24 (2015) 1550092

[Cha01] R. J. Charity et al.:Phys. Rev. C, 63 (2001) 024611

[Cha97] R.J.Charity, M.Korolija,D.G.Sarantites, and L.G.Sobotka, Phys. Rev. C 56, 873 (1997)

[Han87] R. L. Hahn at al.:Phys. Rev. C, 36 (1987)

[Apa06] Aparajiita Dey et al., Phys. Rev. C74, 044605 (2006)

[Coh74] S.Cohen, F.Plasil and W.J.Swiatcki, Ann.Phys(NY) 82,557 (1974)

[Bec01] C.Beck et al, Phys.Rev.Lett C, 63 (2001)

[Vie88] G.Viesti et al. Phys. Rev. C, 38 (1988)

[Tan11] Tange (2011): GNU Parallel - The Command-Line Power Tool, ;login: The USENIX Magazine

[GEM] R.J.Charity, computer code GEMINI (unpublished) URL http://www.chemistry.wustl.edu/∼rc

[Sto81] R.G.Stokstad and E.E. Gross, Phys. Rev. C, 23 (1981)

[Hui89] J.R.Huizenga, A.N. Behkami, I.M. Govii, W.U. Schröder, and Toke, Phys. A401, 142 (1989)

[Var15] E. Vardaci, et al., Phys. Rev. C 92 (2015) 034610

[Hüy16] T. Hüyük, et al., Eur. Phys. J. A 52 (2016) 55, https://doi.org/10.1140/epja/i2016-16055-8

[Vaz84] L.C. Vaz, J.M. Alexander, Z. Phys. A – Atoms and Nuclei 318 (1984) 231

[Din16] A. Di Nitto, et al., Phys. Rev. C 93 (2016) 044602

[Kil92] M. Kildir et al., Phys. Rev. C46, 2264 (1992).

[Lac88] R.Lacey et al., Phys.Rev. C 37 (1988)